UCRL-18332

eg. 2

University of California

Ernest O. Lawrence Radiation Laboratory

STRAIN-ENERGY INTERACTIONS BETWEEN SOLUTE ATOMS AND DISLOCATIONS

Tibor Stefansky
(Ph.D. Thesis)

July 1968

Berkeley, California

DISCLAIMER

UCRL-18332

UNIVERSITY OF CALIFORNIA

Lawrence Radiation Laboratory
Berkeley, California

AEC Contract No. W-7405-eng-48

STRAIN-ENERGY INTERACTIONS BETWEEN SOLUTE ATOMS AND DISLOCATIONS

Tibor Stefansky

(Ph.D. Thesis)

July 1968

TABLE OF CONTENTS

CONTENTS (continued)

STRAIN-ENERGY INTERACTIONS BETWEEN SOLUTE ATOMS AND DISLOCATIONS

Tibor Stefansky

Inorganic Materials Research Division, Lawrence Radiation Laboratory,
Department of Mineral Technology, College of Engineering,
University of California, Berkeley, California

ABSTRACT

The stress required to drive a single dislocation through a fixed array of isotropic stress centers, due to substitutional solute atoms, is calculated using linear elasticity and numerical methods. Cottrell's model of the strain-energy interaction between solute atoms and dislocations is extended by allowing the dislocation to relax to its equilibrium shape in the stress fields of such atoms.

Two new results are obtained. First, a marked concentration dependence of the flow stress is observed only in the very dilute range. And second, the force-displacement diagrams for cutting the stress fields of attractive and repulsive impurity atoms in solution are not identical.

I. INTRODUCTION

The hardening of metals by controlled additions of foreign atoms in solid solution is of great practical interest and it has been extensively studied. At the present time the relative roles of the various solute atom-dislocation interactions responsible for hardening, particularly in substitutional solid solutions, are not fully understood. Nevertheless, a series of recent and well designed experiments,[1-4] on the low temperature deformation mechanisms of several dilute substitutional alloys, seem to indicate that most of the strengthening results from increases in the initial density of dislocations and a lowering of the stacking fault energy upon alloying.

In contrast, however, the theories of Mott and Nabarro[5,6] and subsequent developments of their work[7,8] attribute the hardening to a direct and uniquely different effect, namely the elastic interaction of dislocations with individual solute atoms.* Much of the appropriate experimental data in the literature[8-12] has been interpreted in terms of these theories despite the fact that these data do not identify the specific solute atom effects responsible for the observed strengthening.

It is therefore important to examine closely the dichotomy between the predictions of a Mott and Nabarro type of theory and those experimental results[1-4] which indicate that solute atoms are not the rate controlling barriers to dislocation motion. To this end, we have reformulated the problem of the stress required to drive a dislocation through a fixed

---

* In general, only the strain-energy interaction due to atomic size differences is considered since it is by far the predominant effect.

array of solute atoms without introducing some of the simplifications made in previous analyses. We shall discuss these simplifications later and mention here only their salient features. Thus, it has been customary to regard solute atoms as simple point obstacles and to neglect the equilibrium curvature of a dislocation in the stress field of a solute atom. The result has been, as we shall prove later, to omit important details of the strain-energy interaction between solute atoms and dislocations.

In the present paper, substitutional impurities are regarded as isotropic strain centers and dislocations are treated in the "elastic string" approximation. Within the framework of linear elasticity, and using numerical methods, we allow a dislocation to relax to its equilibrium shape, in the stress field of an array of immobile solute atoms, as the applied stress is increased from zero to the flow stress. We find a flow stress vs. concentration dependence quite different from that predicted by earlier formulations[5-8] and relevant to recent experimental findings.[1-4] We find also that the force-displacement diagrams for cutting solute atom stress fields where the interactions are repulsive are not identical with the case where they are attractive in conflict with Cottrell's[13] simple approach to this problem.

II. SUMMARY OF EARLIER THEORETICAL CONSIDERATIONS

A. The Misfitting-Sphere-in-Hole Model and the Stress Field of a Solute Atom

The elastic behavior of a substitutional impurity can be approximated by the misfitting-sphere-in-hole model described in Appendix I. In this model a spherical cavity of radius r_o is cut in an elastic continuum representing the matrix; an elastic sphere of radius r', representing the impurity atom, is introduced and the surfaces of the two are pulled together and cemented at an equilibrium radius $r = r_o(1 + \epsilon)$, where ϵ is the atomic size misfit.* This process is accompanied by radial displacements only, and as a result it introduces a spherically symmetrical distortion in the lattice.

The strain-energy interaction between the impurity and a dislocation is equal to the elastic work done when the radial displacements take place in the hydrostatic stress field of a dislocation. In the linear elastic approximation a pure screw dislocation has no hydrostatic stress component and therefore spherical solute atoms interact only with the edge components of dislocations. There is nevertheless an elastic interaction between a substitutional impurity and a screw dislocation.[15] It results from the torque that the stress field of the impurity exerts on the dislocation, trying to twist it into an edge orientation where the strain energy interaction can lower its total energy.

For our purposes it will be more convenient to represent the elastic distortions due to impurities by internal stresses in the alloy. In Fig. 1 assume that the x-y plane is the slip plane of an edge dislocation

* An experimental measure of ϵ is provided by $1/a \; da/dc$ where a is the lattice parameter and c is the concentration of solute.

with Burgers vector b in the y-direction and that a solute atom is located at (0,0,h). As shown in Appendix I, this solute atom causes a shear stress in the slip plane, in the direction of b, equal to:

$$\tau_{zy} = 6\, G\, r_o^3 \epsilon \, \frac{yh}{(x^2+y^2+h^2)^{5/2}} \qquad (1)$$

where G is the shear modulus of elasticity. In deriving Eq. (1) we have assumed the elastic constants of solvent and solute to be identical. Since we shall be concerned with dilute solutions this assumption will only be a minor drawback. In addition, we also avoid the questionable practice of assigning different elastic constants to an individual solute atom when these constants are actually determined by the binding forces between large groups of atoms.

If we select the slip plane as the (111) plane in fcc crystals, we obtain $h_1 = \pm b/\sqrt{6}$ for a solute atom on the atomic plane immediately adjacent to the slip plane and $h_2 = \pm 3b/\sqrt{6}$ for a second layer solute atom. As an illustration, we show in Fig. 2 the shear stress contours on the slip plane due to an oversize solute atom at $(0,0,b/\sqrt{6})$. Similarly, we show in Fig. 3 the shear stress profiles at x = 0 due to a solute atom at $(0,0,b/\sqrt{6})$, (curve A), and $(0,0,3b/\sqrt{6})$, (curve B). The figures indicate that a solute atom affects a relatively short length of dislocation, up to 5b or 6b. It is also evident that the shear stress contours vary quite sharply. Consequently, small changes in the curvature of a dislocation in the neighborhood of a solute atom could result in significant changes in the force that the solute atom exerts on the dislocation. Up to the present the force-displacement relationships for cutting the stress fields of solute atoms have been calculated only for the case of rigid, straight dislocations.[8,13]

B. Force-Displacement Diagram for Cutting Spherical Impurities by Straight Edge Dislocations

The interaction energy between an infinitely long edge dislocation and an individual solute atom is also equal to the work done by the elastic forces due to the solute atom when the dislocation is introduced in the crystal. With reference to the dislocation-solute atom geometry of Fig. 1, the elastic interaction energy for a straight dislocation is:

$$U = -\int_{-\infty}^{y}\int_{-\infty}^{\infty} (\tau_{zy} b)\, dx\, dy \qquad (2a)$$

which, when integrated, yields the well known Cottrell interaction energy,

$$U = 4 G r_o^3 \epsilon b \frac{h}{y^2+h^2} \qquad (2b)$$

This expression includes the contributions from both the regions interior and exterior to the impurity.

The force-displacement relationship for cutting the stress field of an isolated solute atom by a long, straight edge dislocation, is obtained by taking the derivative of the interaction energy with respect to position:

$$F = -\frac{\partial U}{\partial y} = -8 G \epsilon r_o^3 b \frac{yh}{(y^2+h^2)^2} \qquad (3)$$

Cottrell[14,16] has pointed out that Eq. (2b) overestimates the interaction energy near the center of the dislocation because of the effects of the core and deviations from Hooke's law. He has suggested that these effects can be taken into account approximately by altering Eq. (2b) to:

$$U = 4 G\epsilon r_o^3 \; b \; \frac{h}{y^2+h^2+\rho^2} \tag{4}$$

where ρ can be thought of as the effective width of the dislocation. At dislocation-solute spacings less than ρ, the only strain energy interaction is with the crystal itself and not with the dislocation. The corresponding force-displacement relation becomes:

$$F = -8 G r_o^3 \epsilon b \; \frac{yh}{(y^2 + h^2 + \rho^2)^2} \tag{5}$$

In principle, the correction term can be found by comparing measured binding energies[9] for substitutional impurities with the predictions of theory [Eqs. (2b) and (4)]. The results, however, are inconclusive as it is difficult to estimate the elastic contribution to the measured energies. A less rigorous but satisfactory choice of ρ can be made on physical grounds. The effects of the correction term on both the interaction energy and the force-displacement diagram should be small at distances roughly in excess of a Burgers vector from the center of the dislocation. In addition, a correction that will reduce the maximum unadjusted force by at least a factor of two appears reasonable.[8] Values of ρ^2 in the range $.06\, b^2 < \rho^2 < .08 b^2$ satisfy these two requirements. For a first layer solute atom at $h = -b/\sqrt{6}$ the choice of $\rho^2 = .07 b^2$ modifies the interaction energy as shown in Fig. 4 and the force-displacement diagram as shown in Fig. 5.

No correction is necessary for second (or higher) layer solute atoms as their distance from the dislocation core is always greater than a Burgers vector. The force-displacement relation for cutting a second

layer atom at $h = -3b/\sqrt{6}$ is also shown in Fig. 5 in order to illustrate the rapid decrease of the maximum force with separation of the impurity from the slip plane.

The core adjustment can be introduced at some other step in the calculations and in a later section we shall be interested in a correction term $f = f(x,y,h,\rho)$ such that:

$$-\int_{-\infty}^{y}\int_{-\infty}^{\infty} (\tau_{zy}b)\, f(x,y,h,\ )\, dx\, dy = 4\, Gr_o^3 \epsilon b\, \frac{h}{y^2+h^2+\rho^2} \qquad (6)$$

We find that Eq. (6) is satisfied numerically when $f = 1-e^{-3(x^2+y^2+h^2)/b^2}$ and $\rho^2 = .07b^2$. The term $f = 1-e^{-3(x^2+y^2+h^2)/b^2}$ provides an empirical correction to the force perunit length of dislocation due to a solute atom* ($F = \tau_{zy}b$) near the core region of the dislocation. The interaction energy corresponding to this new form of the core correction factor is:

$$U = -\int_{-\infty}^{y}\int_{-\infty}^{\infty} (\tau_{zy}b)\left[1-e^{-3(x^2+y^2+h^2)/b^2}\right] dy\, dx \qquad (7)$$

and as shown in Fig. 4, it gives the same result as Eq. (4) with $\rho^2 = .07b^2$. Similarly, the force-displacement relation becomes

$$F = -6\, Gr_o^3\, \epsilon b \int_{-\infty}^{\infty} \frac{yh}{(x^2+y^2+h^2)^{5/2}}\left[1-e^{-3(x^2+y^2+h^2)/b^2}\right] dx \qquad (8)$$

and as demonstrated in Fig. 5, it is equivalent to Eq. (5) with $\rho^2 = .07b^2$.

---

* (or equivalently, the force exerted by the dislocation, per unit length of dislocation, on a solute atom.)

The theories of Mott and Nabarro, and related works, have been formulated in terms of the simple, straight dislocation interactions we have just presented.

C. Mott's and Nabarro's Theory

The first dislocation theory of strengthening due to impurities in solid solution was that of Mott and Nabarro.[5] Starting with the sphere-in-hole model described earlier they calculate that the internal stress at a distance R from the inclusion is approximately

$$\sigma_i = \pm \epsilon G \frac{r_o^3}{R^3}$$

They state further that a dislocation will sweep across its slip plane only if the applied stress is equal to some average of the internal stress in the crystal. One of the problems associated with this approach is the selection of the appropriate average on physical grounds. One way is to state that if impurities are uniformly distributed at a distance λ from each other, the average distance from a point in the matrix to the nearest solute atom is $\lambda/2$ and hence, the mean absolute internal stress is

$$\sigma_o \simeq \epsilon G \left(\frac{2r_o}{\lambda}\right)^3 \simeq \epsilon G c \qquad (9)$$

where c is the atomic fraction of solute. To the approximations of the theory this is the incremental flow stress of the material.

This formulation contains several additional drawbacks. Solute atom-dislocation interactions are not specifically considered and details of the motion of a dislocation through the stress fields of individual solute atoms remain unclarified. Solute atom effects are further thought

to result in a uniform retarding stress on the dislocation and thus yield a long-range stress level. As seen in Figs. 2 and 3, the stress fields of substitutionals act over a limited area of the slip plane and have no tendency to spread as the height of the impurity from the slip plane increases. It is therefore unlikely that individually dispersed solute atoms can result in a long-range stress field. Substitutionals may contribute to long-range stress fields in other ways, as for example, by forming clusters. However, this is not the problem under consideration here.

The theory of Mott and Nabarro has gone through several stages of development and its most advanced formulation is due to Friedel.[7]

D. Friedel's Theory

The improvements of the theory introduced by Friedel[7] are based on the idea that dislocations in the alloy do not move as rigid straight lines. Instead, they tend to be wavy in order to minimize their total energy in the stress fields of the solute atoms. In a random solid solution, one half of the solute atoms adjacent to the slip plane of a dislocation will be attractive and, according to Friedel, the dislocation line will zigzag from one such atom to another. Under these conditions, the flow stress is determined by a balance between the dislocation's tendency to minimize its length and its attraction to solute atoms.

The theory is formulated in terms of the triangular array of solute atoms shown in Fig. 6. A dislocation prefers the zigzag configuration ABC to the straight line configuration Y-Y' as in passing from the latter to the former it gains more in binding energy than it loses in line energy.

The binding energy gained per unit length along Y-Y' is

$$E_1 \simeq \frac{U_B}{y} \simeq \frac{U_B c}{b^2} \; x$$

where U_B is the total binding energy and c is the atomic fraction of solute on the slip plane. Since impurities are regarded as point obstacles, U_B is equal to the maximum absolute value of Eq. (4) or Eq. (7). The increase in the total line energy is

$$E_2 \simeq \frac{Gb^2}{2y} \left[\sqrt{x^2+y^2} \quad -y\right]$$

where $Gb^2/2$ is the dislocation line tension.

By minimizing E_1-E_2 with respect to x, Friedel obtains the triangular distribution that gives the minimum barrier to the moving dislocation. Thus, the flow stress at $0^\circ K$, i.e., the stress required to move the dislocation from a stable position ABC to an equivalent position AB'C is approximately

$$\tau \simeq \frac{1}{2} \; G\epsilon c \qquad (10)$$

The answer, which depends somewhat on the values chosen for the binding energy and the dislocation line tension, is essentially the same as that of Mott and Nabarro (Eq. (9)).

The result is based partly on the arbitrary assumption that the presence of repulsive atoms does not influence the configurations of Fig. 6. And even if dislocations in annealed (and unstrained) crystals were to zigzag from one attractive impurity to another it is not clear why Eq. (10) adequately represents the flow stress. Thus, the dislocation in Fig. 6 will sweep across its slip plane only after cutting some repulsive obstacles, which are not considered, and cutting

additional attractive obstacles which will not always be positioned so as to offer the least resistance to the moving dislocation.

Friedel's answer to these objections is that the cutting of impurities in solution is the same whether they are attractive or repulsive except that it is the attractive impurities that determine the zigzags. We shall question these assertions in our model.

Friedel has also treated the case of an array of repulsive obstacles. The flow stress is now determined by a different criterion, namely that every time an obstacle is cut a new obstacle is met and is approximately equal to

$$\tau \simeq G\epsilon^{3/2} c^{1/2} \qquad (11)$$

The validity of the "steady state" criterion used to determine the flow stress has not been upheld by statistical studies.[20,21]

E. Fleischer's Theory

Fleischer's work[8] is an attempt at erecting a more comprehensive model of solution strengthening in terms of the total elastic interaction between solute atoms and both edge and screw dislocations. The novelty of his approach is not in the theoretical formulation of these interactions but in the way that he uses them to interpret experimental data. Thus, size effects are described in terms of Cottrell's model (cf. section II.2) including a small second order interaction with screw dislocations.[17] The modulus effect,* an exact theoretical treatment

* Solute atoms "softer" than the matrix relax a dislocation's strain field and result in a binding contribution to the elastic interaction energy. The converse is true for solute atoms "harder" than the matrix.

of which appears very difficult, is calculated following an approximate procedure suggested by Eshelby.[18] Inasmuch as an excellent review of Fleischer's work[8] is available, only the final results will be given here.

Fleischer shows that the total elastic force that a spherical impurity exerts on a dislocation is proportional to $e_E = \epsilon_G - 16\epsilon_a$ for an edge dislocation, and to $e_s = \epsilon_G - 3\epsilon_a$ for a screw dislocation. The term ϵ_G measures the modulus misfit ($\epsilon_G = \frac{1}{G}\frac{dG}{dc}$) and ϵ_a the size misfit ($\epsilon_a = \frac{1}{a}\frac{da}{dc}$). Since the hardening is expected to vary with the appropriate force in a simple manner, Fleischer plots $d\tau/dc$, the observed rate of change of the yield stress with composition, as a function of e_E and and e_s. On the basis of such plots for a series of copper alloys, he concludes that screw dislocations control the flow stress since the correlation between $d\tau/dc$ and ϵ_s is very good.

These arguments are not very compelling, however. The flow stresses, obtained from various measurements in the literature, refer to tensile tests on polycrystalline alloys, whereas the critical resolved shear stress for glide in single crystals is a more relevant property. There is considerable scatter in the tensile data and it is not clear whether the specimens were in the same state prior to testing. The latter is an important point as it has been shown[1] that alloying can greatly increase the rate of strain hardening. Fleischer's conclusions are also in conflict with dislocation damping measurements[19] on copper alloy single crystals. These measurements show that the dominant contribution to the binding energy is the strain-energy interaction with edge dislocations.

In contrast with the formulations of Mott and Nabarro and of Friedel, the flow stress on the basis of the Fleischer model is determined by the maximum stress that a dislocation must overcome. If we make the reasonable assumption that size effects predominate, a very simple answer is obtained. Let F_{max} be the maximum force to cut a solute atom at 0°K. Based on the calculations of Sec. IIB, it is shown on Fig. 5 that $F_{max} \simeq 1.17\ Gb^2\epsilon$. Let λ be the spacing of these forces on the slip plane of a dislocation. In general, $\lambda = \frac{nb}{\sqrt{c}}$ where n is the numerical factor that depends on the type of array chosen. Equating the restraining force per unit length of dislocation, F_{max}/λ, to the force per unit length due to the applied stress, tb, we obtain for the flow stress

$$\tau \simeq \frac{1.17}{n}\,\epsilon G c^{1/2} \qquad (12)$$

We will show later on the basis of a more sophisticated model that Eq. (12) has very limited applicability.

III. THE PRESENT THEORETICAL MODEL

A. Idealized Distributions of Solute Atoms

The distribution of solute atoms in an alloy is more or less random.* An exact theoretical treatment of the propagation of a dislocation through a random distribution of solute atoms appears to be very difficult and one must generally resort to regular arrays.

It has been shown[20,21] that the critical applied shear stress required to drive a single dislocation through a random distribution of simple point obstacles can be substantially lower than for a square array of the same density. The discrepancy is greatest for weak obstacles and it can be expected to hold for more complicated examples of weak obstacles such as substitutional solute atoms. There are also differences in the details of dislocation motion through randomly and regularly distributed obstacles. Nevertheless, certain features of the problem, such as the issue of the equilibrium curvature of the dislocation in the stress fields of impurities, can be conveniently illustrated in terms of regular arrays. Such arrays can also be used to study the concentration dependence of the flow stress by introducing an approximate "randomness correction".

A dislocation line in an alloy will, on the average, pass equal numbers of attractive and repulsive obstacles. For this reason array 1, shown on Fig. 7, is of particular interest. In this array a dislocation that is essentially in the edge orientation, with Burgers vector in the y-direction, encounters alternatingly attractive and repulsive solute atoms - a situation which crudely resembles the real case. Array 1 is

---

* We are not concerned here with the problem of impurity clouds along a dislocation or clustering.

but one of many that satisfy these conditions. However, it has the virtue of being among the simplest of such arrays and this is of considerable help in keeping the problem free of ancillary details.

If the dislocation in question is perfectly rigid and straight it will move under a negligibly small applied stress. This has led some authors[22] to suggest that clustering or segregation of solute atoms must occur before strengthening results. The problem is avoided if one considers, as we shall do here, the more realistic case of a flexible dislocation: neighboring sections of the dislocation can now curve and move partly independently of each other so that the internal stress opposing dislocation motion is no longer zero.

We shall use array 1, among others, to study the concentration dependence of the flow stress and as a first approximation consider only solute atoms immediately adjacent to the slip plane.* This is a reasonable approximation since the maximum force to cut second layer solute atoms is quite small (Fig. 5) and we have also indicated (Section II.A) the unlikelihood of such atoms contributing to a long range stress field.

Two other arrays, shown on Figs. 8 and 9, will be considered in this paper. Geometrically, they are identical to array 1 except that all of the obstacles are of the same sign: attractive in array 2 (Fig. 8) and repulsive in array 3 (Fig. 9). By comparing the behavior of arrays 2 and 3, on the one hand, and array 1 on the other, we can test Friedel's assertion that dislocation motion in solid solutions is controlled by

* Throughout this work the slip plane shall refer to the (111) plane in fcc crystals.

attractive obstacles. In addition, arrays 2 and 3 will indicate whether the force-displacement diagrams for cutting attractive and repulsive solute atoms by flexible dislocations are identical.

As noted in Section II.A, the stress field of misfitting solute atoms can be represented by a shear stress on the slip plane of a dislocation. As an example, if the core adjustment factor is introduced as in Eq. (6), for the problem described with reference to array 1 the pertinent shear stress at a point (x,y,0) on the slip plane is

$$\tau_{zy} = 6G\epsilon r_o^3 \sum_i \frac{(y-y_i)h_i \left\{ 1 - e^{-3[(x-x_i)^2+(y-y_i)^2+h_i^2]/b^2} \right\}}{[(x-x_i)^2 + (y-y_i)^2 + h_i^2]^{5/2}} \qquad (13)$$

where (x_i, y_i) are the coordinates of the solute atoms on the atomic planes immediately adjacent to the slip planes and $h_i = \pm b/\sqrt{6}$. In regular arrays these coordinates can be easily determined in terms of a suitable spacing, such as the spacing λ shown in Figs. 7 to 9. λ in turn is fixed by the concentration of solute. Thus, in arrays 1 to 3, the fraction (or concentration) of solute on atomic planes is

$$c = \frac{2}{(\lambda/b)^2} = 2\frac{b^2}{\lambda^2} \qquad (14)$$

where b^2 is taken as the "area" of an atom.

B. Equilibrium Shapes of Dislocations in Arrays of Solute Atoms

A method of calculating the minimum energy configuration of a dislocation in an array of solute atoms is presented in this section. Inasmuch as the same technique applies to all arrays, the calculations for

array 1 will be illustrated in detail and for arrays 2 and 3 only the results will be given.

Despite the symmetry of array 1 many configurations are possible but, as shown in Section III.A, the most interesting ones appear to be those mainly of edge character with Burgers vector in the y-direction. Consequently, we shall restrict ourselves to simple configurations periodic with λ which can result from the relaxation of an edge dislocation, originally along the x-axis, to its minimum energy shape.

In Fig. 10 assume that the edge dislocation in question is displaced from the x-axis to an as yet unspecified (but periodic) shape y(x) by an applied stress τ^* or the internal stresses τ_{zy} or both. The resulting change in the energy of a segment of length λ is approximately

$$U-U_o = \int_{-\lambda/2}^{+\lambda/2} \left\{ \Gamma \left[\sqrt{1 + (dy/dx)^2} - 1 \right] - \int_0^y \tau_{zy} b\, dy - \tau^* b y \right\} dx \tag{15}$$

where the interval $-\lambda/2 \leq x \leq \lambda/2$ was selected for convenience, and Γ is the dislocation line tension. The first term in Eq. (15) represents the increase in total line energy; the second term is the strain-energy interaction of the segment dislocation with the internal stresses τ_{zy} (Eq. 13) and the last term is the work done by the applied stress. The zero of energy, U_o, can be assigned arbitrarily and we shall choose $U_o = 0$.

In writing Eq. (15) the elastic interaction between different parts of the dislocation line has been neglected. This is a reasonable assumption for weak obstacles such as substitutional solute atoms, which will

be cut before the curvature of the dislocation becomes appreciable. The validity of this assumption has been upheld by recent computer studies[23] of the bowing of a dislocation segment. These studies have also confirmed the adequacy of the "elastic string" model of a dislocation in the case of weak obstacles provided that the line tension appropriate to the orientation of the dislocation is used. In the linear elastic approximation, spherical solute atoms constitute obstacles to the edge components of dislocations only and therefore, the appropriate line tension is

$$\Gamma = \Gamma_{edge} \simeq \frac{3}{4} Gb^2 \qquad (24)$$

The problem now is to find the shape y(x) of the segment which minimizes its energy U. From the calculus of variations it is known that if y(x) is to minimize the integral (15) it must satisfy the Euler equation

$$\frac{d}{dx}\left(\frac{\partial U}{\partial p}\right) - \frac{\partial U}{\partial y} = 0$$

where $p = dy/dx$. The result of performing the indicated operations is

$$\frac{d^2y/dx^2}{[1 + (dy/dx)^2]^{3/2}} = -\frac{b}{\Gamma}(\tau^* + \tau_{zy}) \qquad (16a)$$

which can be recognized as the differential form of the equation for the equilibrium radius of curvature. The negative sign was chosen to make the curvature positive when y(x) is concave upwards.

For the purpose of computation it is more convenient to use Eq. (16a) in the dimensionless form

$$\frac{d^2y'/dx'^2}{[1+(dy'/dx')^2]^{3/2}} = -\frac{4}{3}\left(\frac{\lambda}{b}\right)\left(\frac{\tau^*}{G}+\frac{\tau_{z'y'}}{G}\right) = -\left\{\frac{4\sqrt{2}\,\tau^*}{3\sqrt{c}\,G}\right.$$

$$\left. + \frac{\epsilon c}{2}\sum_i \frac{(y'-y_i')h_i'\left[1-e^{-6\{(x'-x_i')^2+(y'-y_i')^2+h_i'^2\}/c}\right]}{\left[(x'-x_i')^2+(y'-y_i')^2+h_i'^2\right]^{5/2}}\right\} \qquad (16b)$$

where the line tension has been set equal to $3/4\ Gb^2$ and the primes denote quantities dimensionless in λ. The parameter λ represents the period of the alloy lattice as shown in Eq. (14) it is related to the atomic fraction of solute by $\lambda = \sqrt{2}\ bc^{-1/2}$.

Equation (16a or 16b) is a second order non-homogeneous differential equation which can be solved numerically upon specifying two independent boundary conditions. There is an infinite number of pairs of such conditions and for each of them it is possible to obtain a minimum energy line shape $y'(x')$. However, only solutions which are symmetric about the y-axis and with period λ are being considered here. From the symmetry, we can conclude that $dy'(x')/dx' = 0$ at each solute atom, and this is one of the boundary conditions. The composition c, the size misfit ϵ and the reduced applied stress τ^*/G appear as constants in Eqs. (16) and each set requires a separate solution. The computations, described in Appendix II, were performed on a CDC 6600 computer using

the Adams method.[25] This method involves step-by-step solution over the chosen interval $-1/2 \leq x' \leq 0$* and it requires that the initial conditions be known at the starting point $(-1/2, y'_o)$. For array 1 these are: $dy'/dx'\big|_{x' = -1/2} = 0$ and a y'_o in the range $0 \leq y'_o \leq 1/2$. Different line shapes are obtained for each y'_o but only those with period λ, and having zero slope at $x' = 0$, are of interest here. These line shapes can be found by plotting (for each c, ϵ, and τ^*/G) the calculated slope at $x' = 0$ as a function of y'_o.

Following Friedel's approach we consider first the equilibrium configurations in the absence of an applied stress ($\tau^*/G = 0$). To illustrate this case we use $\epsilon = 0.06$ and $c = 0.00125$ which are within the range that Friedel states as representative in his formulation.[9] As shown on Fig. 11 there exist four line shapes (corresponding to $y'_o = 0$ or 1/2, 0.0026, 1/4 and 0.4841) compatible with the periodicity condition and they are sketched on Fig. 10 (curves a,b,c and d, respectively). Each of these configurations $y'(x')$ minimizes the energy U, according to Eq. (15), but the most stable one will have the smallest "minimum" energy. Figure 12, where U is plotted as a function of y'_o, indicates that configuration "d" (or its mirror image "b") is the most stable. An accurate drawing of line shape "d" is given on Fig. 13 to show the actual deviation of the dislocation from a straight line. The identical configurations "a" and "c" are unstable and have zero energy in agreement with $U_o = 0$.

Similar configurations prevail under a finite applied stress. This is illustrated in Figs. 10-12 for $\tau^*/G = .001$. The lowest energy shape is

* The line shapes are symmetric about the y-axis, hence only half the period need be considered.

again "d" and as shown in Fig. 11 this is the only possible type of configuration when $\tau^*/G > .00124$. The higher applied stress required to make configuration "d'" unstable will later be shown as due to the stronger strain-energy interaction between repulsive solute atoms and flexible dislocations. The two other line shapes (at $\tau^*/G = .001$) for which $dy'/dx'|_{x'=0} = 0$ are unstable and they correspond to a position of the dislocation on the descending portion of the internal stress curve (Fig. 3).

There is no essential change in the details of Figs. 10-13 over the whole range of composition ($0 < c \leq .16$) and atomic size misfit ($.20 \leq \epsilon \leq .10$) studied in this paper. In array 1, therefore, the quilibrium shape of a dislocation line is wavy but the waviness is not in the form of zigzags from one attractive obstacle to another.

In arrays 2 and 3, when $\tau^*/G = 0$, only straight line configurations are compatible with the periodicity requirement. In array 2, where all the solute atoms are attractive, the minimum energy shape is a straight line along the x-axis. Similarly, in array 3 where all the obstacles are repulsive a straight line along $y' = 1/4$ has the least energy. Equilibrium configurations under an applied stress are sketched in Figs. 8 and 9.

More detailed information on dislocation line shapes in the neighborhood of solute atoms will be presented later in connection with the force-displacement diagrams. At this stage, however, it can be stated that Friedel's model of dislocation lines in alloys, as zigzags joining attractive obstacles, is not generally valid.

the solute atom. Choosing $c = .01$ and $\epsilon = .06$, as an example, the result of evaluating Eq. (17) over all stable line shapes $y(x)$ is shown by curve i of Fig. 16 as a function of displacement from the solute atom. For a curved dislocation this displacement is not uniquely defined and we have taken it as the distance of closest approach between the solute atom and the dislocation.

A similar calculation for an attractive atom in array 2 yields curve ii of Fig. 16. To the accuracy of the present computations, this latter result is identical to that obtained by Cottrell for an infinitely long and rigid dislocation. This was expected from the agreement between the calculated flow stress for array 2 and the predictions of Fleischer's theory.

The corresponding force-displacement diagrams are obtained by taking the derivative (graphically, in this case) of the interaction energy with respect to distance from the obstacle and they are shown on Fig. 17. Only the ascending branch of the force-displacement diagram can be calculated this way. There are no equilibrium line shapes* of the dislocation for displacements on the descending branch even if the stress is reversed.

A greater maximum force is required to cut a repulsive solute atom at $0^{\circ}K$ and this can be understood with reference to the shape of the internal shear stress contours by which solute atoms oppose the motion of dislocations. Only the ascending portions of the internal shear stress contours are effective in arresting the motion of a dislocation and as shown in Figs. 2 and 3, they vary quite rapidly for attractive atoms and are

* In arrays 2 and 3, the flow stress is reached when the applied stress is just large enough to push the dislocation past the peak of the opposing internal shear stress.

broader, varying more slowly, for repulsive ones (changes in ϵ alter the height but not the shape of these contours). For a fixed value of the applied stress a dislocation can therefore bend more sharply in the opposing stress field of an attractive solute atom than of a repulsive one. The ultimate effect is that the critical curvature, at which the force on a solute atom due to the line tension of the dislocation exceeds the maximum opposing force, is reached at a lower value of the applied stress for attractive atoms. This is illustrated on Fig. 18 where the equilibrium radius of curvature at each type of obstacle is plotted as a function of the applied stress (as before, $c = .01$ and $\epsilon = .06$).

It was shown in Section IV.C that the maximum force to cut a repulsive solute atom varies with the concentration but, as we see in the present section, the computations involved in determining a force-displacement diagram are cumbersome and time consuming. Fortunately, it is possible to arrive at an empirical relationship for the maximum force in terms of the flow stress vs concentration curves that have already been calculated.

For a given value of ϵ, the results on Fig. 15 indicate that

$$\left(\frac{\tau^*}{G}\right)_3 - \left(\frac{\tau^*}{G}\right)_2 = K(\epsilon,c) \tag{18}$$

where $(\tau^*/G)_3$ and $(\tau^*/G)_2$ are the flow stresses for arrays 3 and 2 respectively, and $K(\epsilon,c)$ is a numerical factor which can be read from each set of curves and which depends on ϵ and c. Let the maximum force to cut a repulsive solute atom be denoted by $F^R_{max}(\epsilon,c)$. In array 3, equating the restraining force per unit length of dislocation to the force per unit length due to the applied stress we obtain

$$\left(\frac{\tau^*}{G}\right)_3 = \frac{F^R_{max}(\epsilon,c)}{\sqrt{2}\ Gb^2}\ c^{1/2} \tag{19}$$

For array 2, on the other hand, which behaves according to the Fleischer theory we have

$$\left(\frac{\tau^*}{G}\right)_2 = .827\ c^{1/2} \tag{20}$$

Substituting Eqs. (19) and (20) into (18) we arrive at the final result

$$F^R_{max}(\epsilon,c) = \frac{\sqrt{2}\ Gb^2\ K(\epsilon,c)}{c^{1/2}} + 1.17\ Gb^2\epsilon$$

or

$$F^R_{max}(\epsilon,c) = \frac{\sqrt{2}\ Gb^2\ K(\epsilon,c)}{c^{1/2}} + F^A_{max} \tag{21}$$

Where F^A_{max} is the maximum force, at 0°K, to cut an attractive solute atom.

It is also seen on Fig. 15 that for each ϵ there is a concentration range $c > c_o$ where K is independent of concentration and a range $c < c_o$ where K decreases rapidly with decreasing concentration. $F^R_{max}(\epsilon,c)$, therefore approaches F^A_{max} gradually at high concentrations and rapidly at very low concentrations. This is confirmed in Fig. 19 where the critical (or "cutting") radius of curvature at a solute atom (in arrays 2 and 3) is shown as a function of concentration. As determined by c_o, there is little change in the critical curvature in the concentration range of practical interest.

IV. DISCUSSION OF RESULTS

A. The Flow Stress

It is commonly known that the hardness of a crystal containing inclusions (G.P. zones or precipitates) can vary strongly with their state of dispersion. Several authors[16,26] have speculated that somewhat analogous effects should be apparent in solid solutions and this is precisely what is observed on Fig. 14. At low concentrations, where the spacing of solute atoms is large, the curvature of the dislocation is such that there is an appreciable internal stress opposing its motion. As the spacing of solute atoms decreases, the dislocation becomes straighter because of its finite line tension. The internal stresses along its length now begin to cancel out and it can therefore move at a lower applied stress.

This explanation is confirmed by the calculated effects of changing the spacing of solute atoms on the shape of the dislocation line at the flow stress.* This is shown on Fig. 20a for $\epsilon = .06$. Along u1 ($\lambda = 28.28b$) the shear stresses from all three solute atoms A, B, and C oppose dislocation motion; along u2 ($\lambda = 20b$) atom B has little effect while A and C act as before; finally, along u3 ($\lambda = 7.07b$) the shear stresses from B are in the direction of the applied stress and only A and C are opposing.

It was mentioned in Section III.B that in array 1 there can exist another stable configuration, designated as "b" on Fig. 10, which becomes

---

* The flow stress of array 1 was defined in Section III.B as the stress at which the configuration designated as "d" on Fig. 10 became unstable.

unstable at lower stress. The breakaway stress for configuration "b" is shown in Fig. 21 in comparison with the flow stress ($\epsilon = .06$).* The reasons why configuration "b" is weaker than "d" are twofold. First, a smaller force is required to cut attractive solute atoms. Second, the equilibrium shapes for "b" are such that cancellation of internal stresses along the dislocation takes place at a lower applied stress. The dislocation line shapes are illustrated in Fig. 20b (in each case for the breakaway stress) and the accompanying explanation is the same as for Fig. 20a.

Rather different results are obtained when the solute atoms in array 1 are no longer regarded as isotropic stress centers but simply as attractive and repulsive point obstacles. A flexible dislocation which moves up to contact the line of point obstacles ...ABC..., in Fig. 20a, will bow out between each of them. On the other hand, if the dislocation originally (i.e., at zero stress) lies along the line of obstacles ...BCD..., in Fig. 20b, it will bow out between the attractive ones and ignore the repulsive ones. If the force-displacement diagrams for attractive and repulsive solute atoms are assumed to be identical, the Fleisher model applies directly to both the above situations. The flow stress as given by that model is shown on Fig. 21 in comparison with the results of Section III.C.

---

* Increasing the value of ϵ results in stronger obstacles, between which the bowing of the dislocation can be more pronounced, and therefore the effects of "straightening" appear at smaller solute spacings.

In contrast, the results for array 2 are the same whether solute atoms are treated as isotropic stress centers or as point obstacles and much the same for array 3 if the maximum force to cut a repulsive atom is taken from Eq. (21). Therefore, in the approximation of point obstacles the same flow stress vs. concentration relationship is obtained for all three arrays* provided that the appropriate spacing of solute is chosen in each case (in array 1 the separation of obstacles on the slip plane is half of that in arrays 2 and 3). Perhaps this explains in part why previous authors have described solid solutions in terms of arrays of obstacles that are all of the same sign - in the limit of point obstacles there is no essential difference whether they are attractive or repulsive or some of each.

On physical grounds, however, it is not particularly realistic to consider that a dislocation line in a solid solution is always anchored by a row of attractive impurities or opposed by a row of repulsive ones. In fact, we are going to show, by comparing our results with experimental data, that array 1 adequately describes the average environment of a dislocation line in an alloy and that the behavior shown in Fig. 14 is also characteristic of a random solid solution.

The flow stresses that we have calculated as yet overestimate the strengthening due to strain-energy interactions. It has been shown elsewhere[20,21] that the yield stress for a random distribution of point obstacles can be considerably smaller than for a square array of the same composition. The discrepancy is large for weak obstacles and it

* We neglect the trivial case of a perfectly rigid and straight dislocation.

increases rapidly in the range of strengths corresponding to substitutional atoms. There exists the unfortunate coincidence that the maximum in the force-displacement diagram occurs very near (0.3b) the center of the dislocation where Hooke's law is seriously in error. We have estimated this maximum force to be roughly $1.2Gb^2\epsilon$ by compensating for the effects of the core as described in Section II.B. Most authors[9] evaluate the binding energy at an arbitrary cut-off radius of 1b from the center of the dislocation and arrive at a maximum force approximately an order of magnitude lower than $1.2Gb^2\epsilon$. In the absence of more specific knowledge about the core of the dislocation it is difficult to be rigorous about the adjustment factor and we have very likely erred by underestimating it. In the range of strengths that are customarily attributed to substitutional impurities, $.12Gb^2\epsilon \leq F_{max} \leq 1.2Gb^2\epsilon$, the randomness correction can vary between a factor of 5 and 12. Assuming that this correction also can be used for our problem we find that the flow stresses in Fig. 14 may be too large by a total factor (core and randomness) between 5 and 120. This is not an ad hoc correction but arises from the lack of rigorous and quantitative knowledge about the effects of the core and the statistical features of the problem.

The greatest hindrance to a proper comparison between our theoretical predictions (and those of others) and experimental data lies in the difficulty of separating the contributions of the various solute atom effects which cause the observed strengthening. A notable exception is the recent data of T. Suzuki[27] on the low temperature deformation mechanisms of dilute Cu-Ni single crystals. The distinguishing feature of his work

is that the density of grown-in dislocations in all his crystals was about 10^4 cm^{-2}, which is four or five orders of magnitude lower than in other experimental data. By studying the details of dislocation motion, using etch-pit and stress pulse loading techniques, Suzuki has presented compelling evidence that the rate controlling (thermal) barriers at low temperatures ($< 240°K$) are randomly dispersed solute atoms. The critical resolved shear stress (less the long range or athermal stress) at $4.2°K$ as measured by him is shown in Fig. 22 in comparison with the results of our model where we have chosen a very modest factor of 10 as the randomness (and core) correction.

The agreement both quantitatively and, what is more relevant, qualitatively is very good and it confirms the basic feature of our model, namely that in substitutional alloys the strengthening due to the size effect is confined to the dilute range. We believe further that this behavior is also characteristic of other substitutional alloys but that it has not been observed because the initial densities of dislocations are so large as to make the intersection mechanism in fcc metals the controlling one.

In this respect, another example of interesting experimental data is the early work of Linde and Edwardson[10,11] on the CRSS of Cu-Si single crystals. These data have been conflictingly interpreted by Friedel[7] as due to the size misfit interaction with edge dislocations and by Fleischer[8] as due to the modulus interaction with screw dislocations. More recently, however, Evans and Flanagan[4] have demonstrated by means of activation parameter measurements that the intersection mechanism controls the flow stress of Cu-Si single crystals.

Most of the strengthening is shown to arise from the increased dislocation density due to alloying,* and they obtain a maximum energy to effect intersection that is an order of magnitude larger than the binding energy between a Si atom and an edge dislocation. In this work, as well as in that of Linde and Edwardson, the initial density of dislocations was about five orders of magnitude higher than in Suzuki's experiment and direct solute atom effects are obscured in the background.

The apparent success of the formulations of Friedel and Fleischer in accounting for the Cu-Si data seems therefore to be fortuitous as they overestimate the effects of elastic interactions. As an illustration we also show on Fig. 22, for Cu-Ni, the appropriate predictions of Friedel according to Eq. (11) and of Fleischer [Eq. (9) of Ref. 8], the latter including both the size and modulus effects with edge dislocations. Although their results could be scaled down by some correction factor, they nevertheless do not predict the observed concentration dependence of the flow stress.

B. The Force-Displacement Diagram

A comprehensive discussion of the differences in the maximum force required to cut attractive and repulsive substitutional atoms has already been given in Section III.D.

It is reasonable to assume that equilibrium computations, of the type we have performed in this paper, would result in greater corrections to the force-displacement relationships and interaction energies of

* Unfortunately, it is not possible to estimate from their data the effects of direct solute atom-dislocation interactions.

interstitial impurities and other strong tetragonal defects. The asymmetries in the stress fields of tetragonal distortions are considerably more pronounced than those of spherical distortions but the problem is also more complicated as the elastic interactions between the arms of the dislocation at the defect must now be taken into account.

V. CONCLUSIONS

a) In contradiction with Cottrell's simple straight dislocation model, the force-displacement diagrams for cutting the stress fields of attractive and repulsive solute atoms are not identical, when the equilibrium curvature of the dislocation in the vicinity of the solute atom is taken into account. A greater maximum force at 0°K is required to cut repulsive solute atoms as their effective opposing stress field is broader than that of attractive atoms.

b) The contribution of the size effect to the strengthening of substitutional solid solutions cannot be properly described in terms of the cutting of simple point obstacles even if what is taken as the strength of these obstacles is not seriously in error. Instead, it is necessary to consider in greater detail the strain-energy interaction of the dislocation with the stress fields of the solute atoms and to compute the minimum energy shape of the dislocation line. The opposing internal stress along the dislocation line can be considerably less when the latter is allowed to relax to its equilibrium shape.

As the spacing of solute atoms decreases the dislocation line straightens out rapidly and therefore a marked concentration dependence of the flow stress is observed in the dilute range only. This assertion, which is in conflict with existing theories, is confirmed by experimental data in which the effects of direct solute atom-dislocation interactions have been successfully isolated.

APPENDIX I.

A. The Misfitting-Sphere-in-Hole Model

A spherical hole of radius r_o is cut in the matrix, a sphere of radius $r' = r_o$ representing the solute atoms is introduced and the two are cemented together at an intermediate radius $r_o(1 + \epsilon)$. The impurity and the matrix are treated as classical elastic media.

By definition, if u is the radial displacement, the strains are

$$\epsilon_{rr} = \frac{\partial u}{\partial r}$$

and

$$\epsilon_{\theta\theta} = \epsilon_{\phi\phi} = \frac{u}{r}$$

From the generalized form of Hooke's law we obtain for the stresses

$$\sigma_{rr} = \frac{E}{(1+\nu)(1-2\nu)} \left[2\nu \frac{u}{r} + (1-\nu) \frac{\partial u}{\partial r} \right]$$

and

$$\sigma_{\theta\theta} = \sigma_{\phi\phi} = \frac{E}{(1+\nu)(1-2\nu)} \left(\frac{u}{r} + \nu \frac{\partial u}{\partial r} \right)$$

where E is Young's modulus and ν is Poisson's ratio. By performing a force balance on a differential volume element $r^2 \sin\theta dr\, d\phi\, d\theta$ one arrives at the differential equation for the displacements:

$$\frac{\partial u}{\partial r} + \frac{2u}{r} = C \qquad (1A)$$

where C is a constant independent of r. A solution of Eq. (1A) is

$$u = Ar + \frac{B}{r^2}$$

where Ar is the displacement inside the spherical inclusion and B/r^2 is the displacement in the surrounding matrix.

The constants A and B are determined by equating the displacements at the boundary $r = r_o(1 + \epsilon)$ of the inclusion and thus are $A = \epsilon$ and $B = r_o^3\epsilon$. Assuming that the elastic constants of the inclusion and the matrix are identical, the stresses in the matrix from the generalized Hooke's law are

$$\sigma_{rr} = -\frac{4G\epsilon r_o^3}{r^3}$$

and

$$\sigma_{\phi\phi} = \sigma_{\theta\theta} = \frac{2G\epsilon r_o^3}{r^3}$$

$G = E/2(1 + \nu)$ and $r \geq r_o(1 + \epsilon)$.

B. The Internal Shear Stresses on a Plane

With reference to Fig. A1 assume that a solute atom is located at the origin and that the slip plane of interest is parallel to the x-y plane and at a height z above it. The components of σ_{rr}, $\sigma_{\theta\theta}$, and $\sigma_{\phi\phi}$ in any direction are easily obtained and, as an example, the shear stress τ_{zy} on this slip plane is

$$\tau_{zy} = \sigma_{rr}\left(\frac{z}{r}\right)\left(\frac{y}{r}\right) - \sigma_{\theta\theta}\left(\frac{z}{r}\right)\left(\frac{y}{r}\right)$$

or, in cartesian coordinates:

$$\tau_{zy} = -6G\, r_o^3\epsilon\, \frac{zy}{(x^2 + y^2 + z^2)^{5/2}} .$$

APPENDIX II.

A. Line Shape Computations

The desired set of parameters c, ϵ and τ^*/G are specified and at the starting point of the solution (x_o', y_o'), where $dy'/dx'|_{x_o'} = 0$, the computer is first made to calculate d^2y'/dx'^2 from the equilibrium equation for the radius of curvature. The next value of y', at $x' = x_o' + \Delta x'$, is calculated using a power series expansion

$$(y')_{x_o'+\Delta x'} = y_o' + \left(\frac{dy'}{dx'}\right)_{x_o'} \Delta x' + \frac{1}{2}\left(\frac{d^2y'}{dx'^2}\right)_{x_o'} (\Delta x')^2$$

and

$$\left(\frac{dy'}{dx'}\right)_{x_o'+\Delta x'} = \left(\frac{dy'}{dx'}\right)_{x_o'} + \left(\frac{d^2y'}{dx'^2}\right)_{x_o'} \Delta x$$

where $\Delta x'$ is a suitably small interval, usually taken as .001.

This procedure is repeated for the next two intervals $\Delta x'$ after which the remaining values of y', i.e., those needed to cover a period λ, are calculated from the Adams technique formula

$$(y')_{x_o'+n\Delta x'} = (y')_{x_o'+(n-1)\Delta x'} + \left[2.2917\left(\frac{dy'}{dx'}\right)_{x_o'+(n-1)\Delta x'}\right.$$

$$\left. - 2.4583\left(\frac{dy'}{dx'}\right)_{x_o'+(n-2)\Delta x'} + 1.5417\left(\frac{dy'}{dx'}\right)_{x_o'+(n-3)\Delta x'} - .3750\left(\frac{dy'}{dx'}\right)_{x_o'+(n-4)\Delta x'}\right]\Delta x'$$

At each step $(y', x_o'+n\Delta x')$ of the calculations it is necessary to know $\tau_{z'y'}$ and therefore the coordinates of the solute atoms are arranged in order of increasing distance from $(y', x_o' + n\Delta x')$ and the contributions

of each atom to the internal shear stress are added until further additions are less than .1% of the total.

The energy of a small segment of dislocation between $(n - 1)\Delta x'$ and $n\Delta x'$ is computed from

$$\frac{U}{Gb^3} = \sqrt{\frac{2}{c}} \left[\frac{3}{4} \left(\sqrt{1+\left(\frac{dy'}{dx'}\right)^2_{x'_o+n\Delta x'}} - 1 \right) - \sqrt{\frac{2}{c}} \int_0^{y'} \frac{\tau_{z'y'}}{G} dy' - \frac{\tau^*}{G} \sqrt{\frac{2}{c}}\, y' \right] \Delta x' \tag{2A}$$

and the total energy of a periodic length λ of dislocation line is obtained by adding the energies of all such small segments. The integration indicated in Eq. (2A) is performed by a separate computer routine based on Simpson's Rule.

By reducing the size of the interval $\Delta x'$, the line shapes and energies can be obtained to any desired accuracy.

ACKNOWLEDGMENTS

The author is greatly indebted to Professor John E. Dorn for his kindly and ever informative advice.

This research was performed under the auspices of the United States Atomic Energy Commission.

REFERENCES

1. S. K. Mitra and J. E. Dorn, Trans. AIME 224, 1062 (1962).
2. A. A. Hendrickson and M. E. Fine, ibid. 221, 967 (1961).
3. T. J. Koppenaal and M. E. Fine, ibid. 224 , 347 (1962).
4. K. R. Evans and W. F. Flanagan, Phil. Mag. 16, 535 (1968).
5. N. F. Mott and F. R. N. Nabarro, Report on Conference of Strength of Solids, Phys. Soc., (London), 1948, p. 1.
6. N. E. Mott, Imperfections in Nearly Perfect Crystals, W. Shockley, editor, (John Wiley and Sons, Inc., New York, 1952).
7. J. Friedel, in Dislocations (Addison-Wesley Pub. Co., New York, 1964), Chapter 12.
8. R. L. Fleischer, in Strengthening of Metals, D. Peckner, editor (Reinhold Press, New York, 1964), Chapter 4.
9. N. F. Fiore and C. L. Bauer, Prog. in Mat. Sci. 13, 2 (1967).
10. J. O. Linde, B. Lindell and C. H. Stade, Arkiv f. Fysik 2, 89 (1949).
11. J. O. Linde and S. Edwardson, Arkiv f. Fysik 8, 511 (1954).
12. J. Garstone and R. W. K. Honeycombe, Dislocations and Mechanical Properties of Crystals (John Wiley and Sons, Inc., New York, 1957).
13. A. H. Cottrell, Dislocations and Plastic Flow in Crystals (Oxford Press, Oxford, 1958), p. 56.
14. Ibid., p. 35.
15. W. T. Read, Dislocations in Crystals (McGraw-Hill Book Co., New York, 1953).
16. A. H. Cottrell, Relation of Properties to Microstructure (ASM, Cleveland, 1954).

17. H. Stehle and A. Seeger, Z. Phys. 146, 217 (1956).

18. J. D. Eshelby, Acta. Met. 3, 487 (1955).

19. E. C. Oren, N. F. Fiore and C. L. Bauer, Acta Met. 14, 245 (1966).

20. A. J. E. Foreman and M. J. Makin, Phil. Mag. 14, 911 (1966).

21. J. E. Dorn, P. Guyot, and T. Stefansky, in Physics of Strength and Plasticity, (The Orowan 65th Anniversary Volume), ed. A. S. Argon (M.I.T. Press, Cambridge, Mass., in press).

22. E. D. Levine, et al., Trans. AIME 215, 521 (1959).

23. A. J. E. Foreman, Phil. Mag. 15, 1011 (1967).

24. J. E. Dorn, Energetics of Dislocation Mechanisms, N.R.C. Seminar on Energetics in Metallurgical Phenomena, Denver, Colorado, 1962.

25. F. B. Hildebrand, Advanced Calculus (Prentice Hall Company, New York, 1957).

26. J. E. Dorn, private communication.

27. T. Suzuki, Dislocation Dynamics, (McGraw-Hill Book Company, New York, in press).

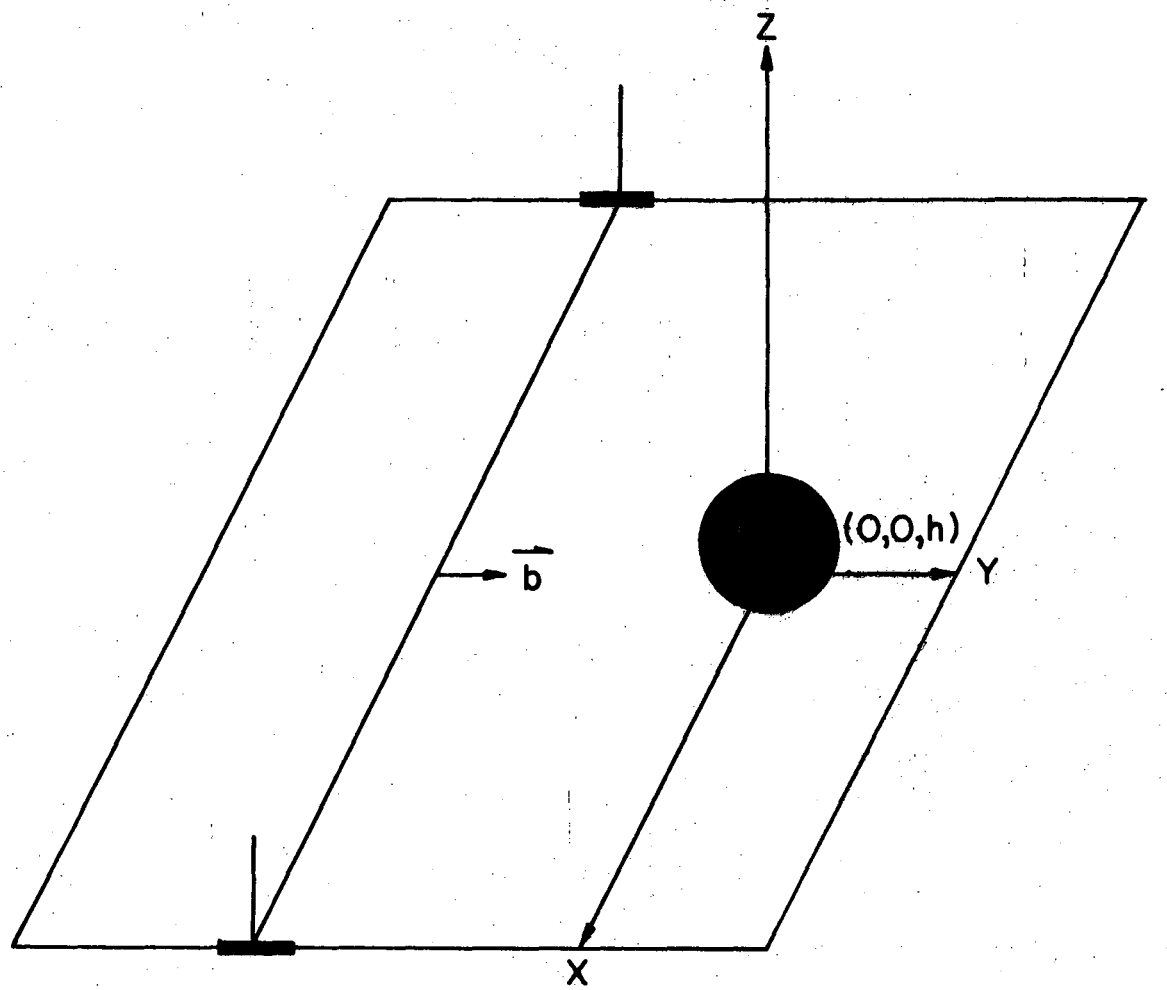

XBL 687-1402

Fig. 1 Solute atom-dislocation geometry

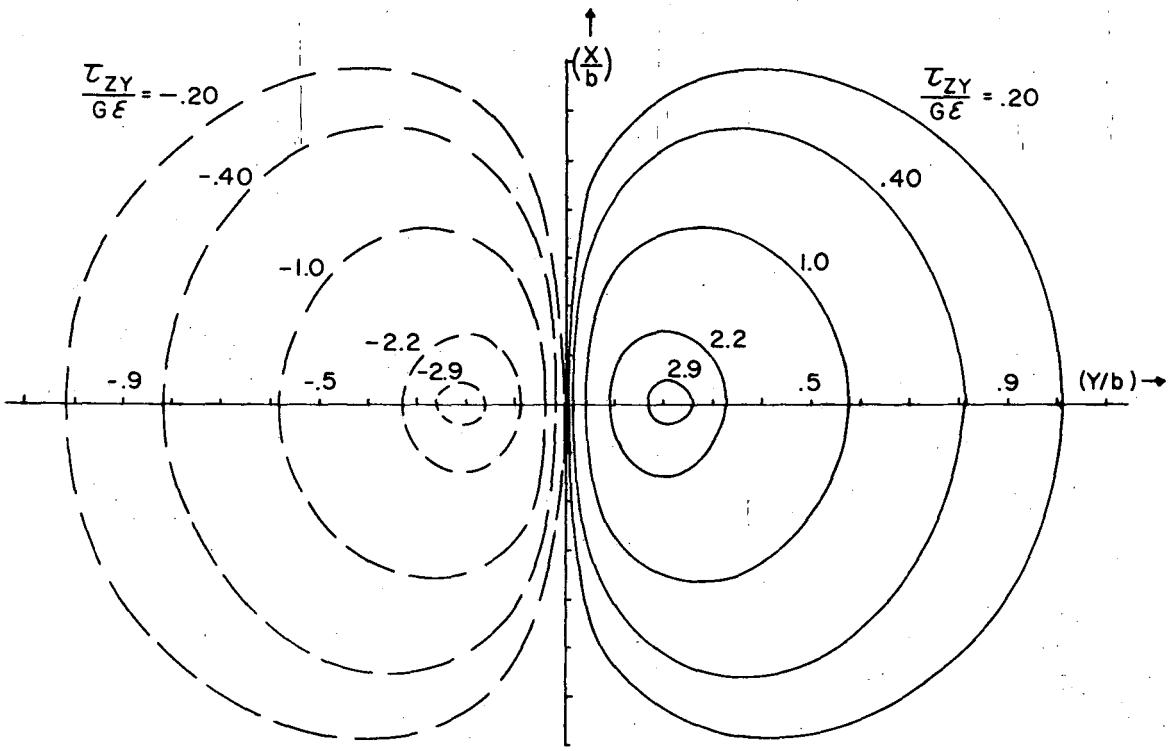

XBL 687-1404

Fig. 2 Internal shear stress contours on the slip plane at X = 0

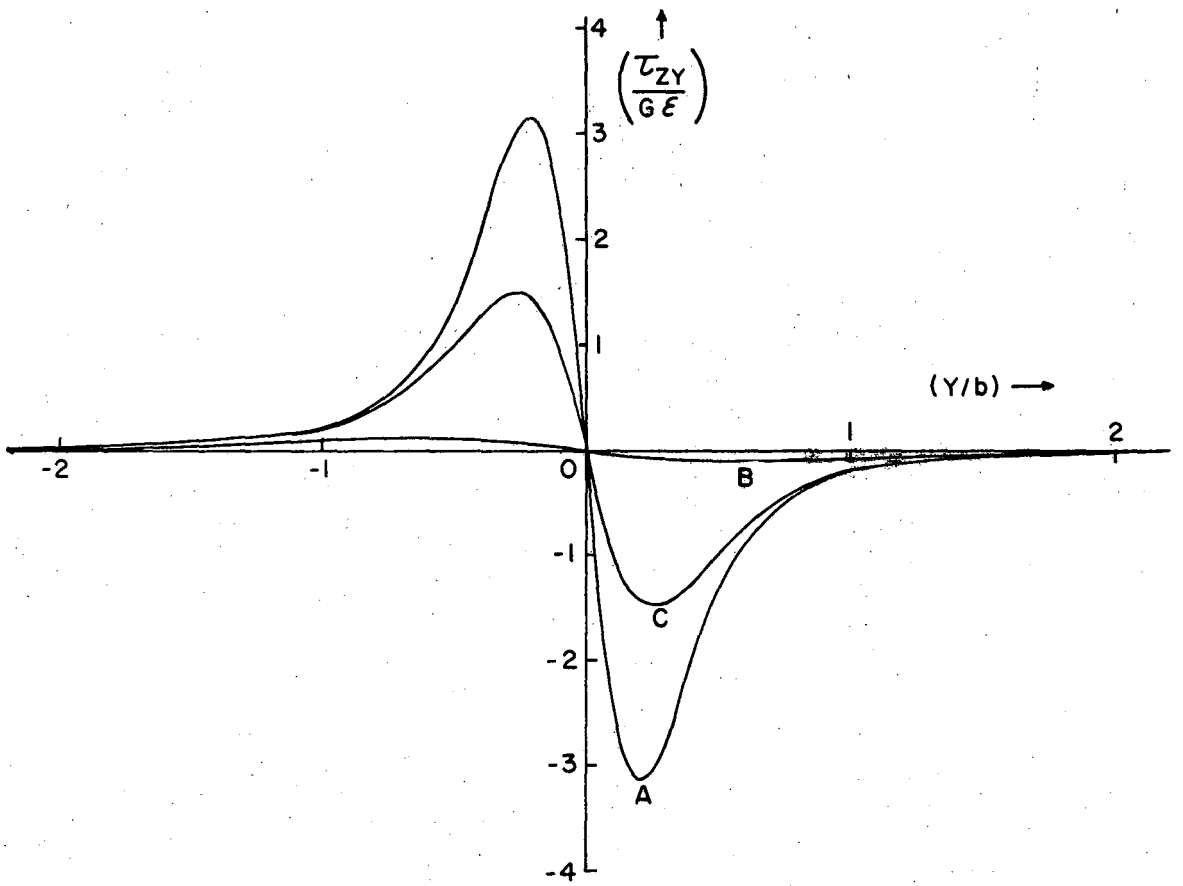

XBL 687-1413

Fig. 3 Internal shear stress profiles

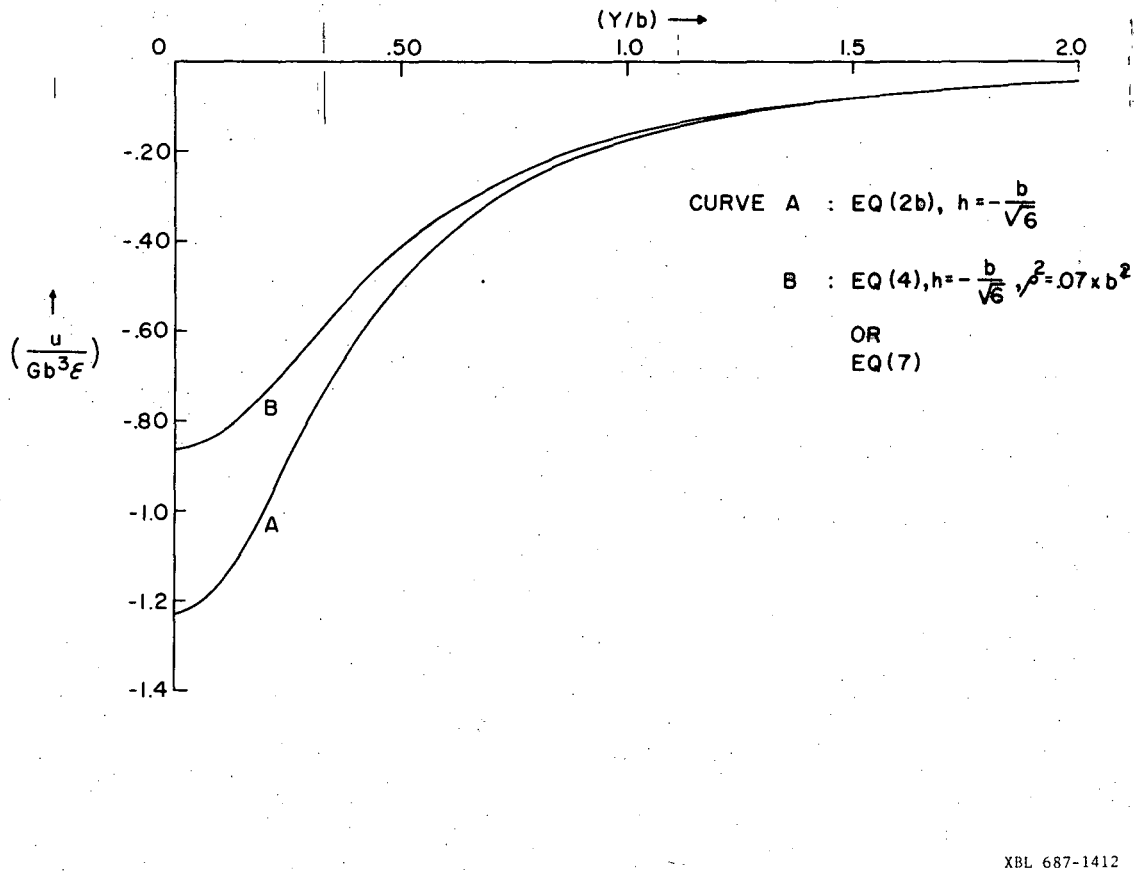

Fig. 4 Strain energy interaction for rigid dislocations

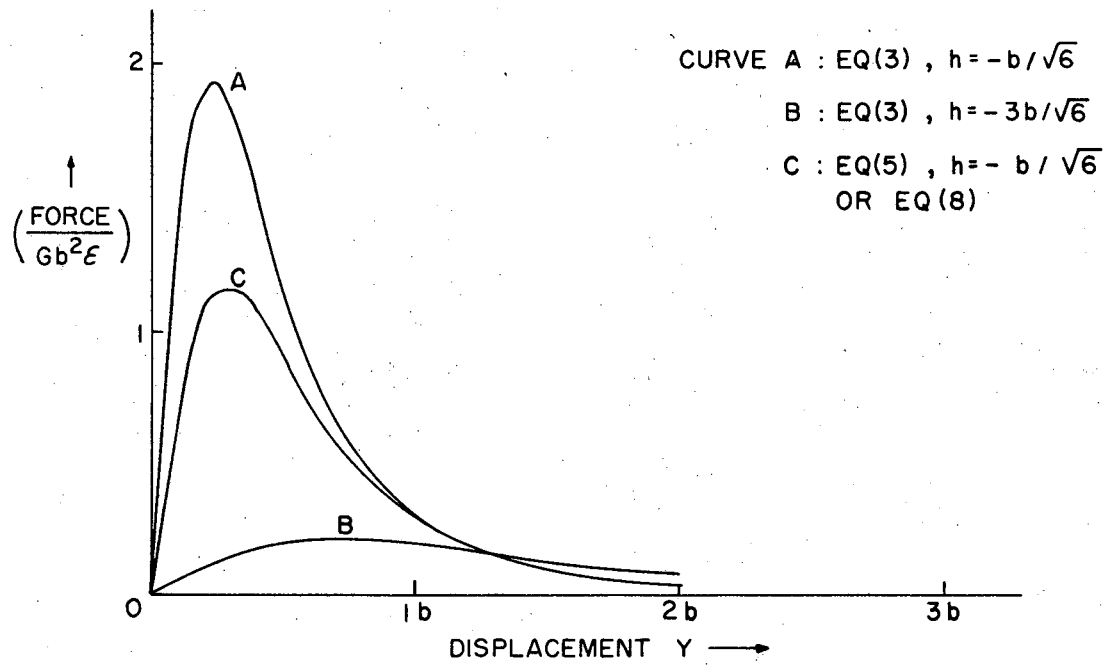

XBL 687-1403

Fig. 5 Force-displacement diagrams for rigid dislocations

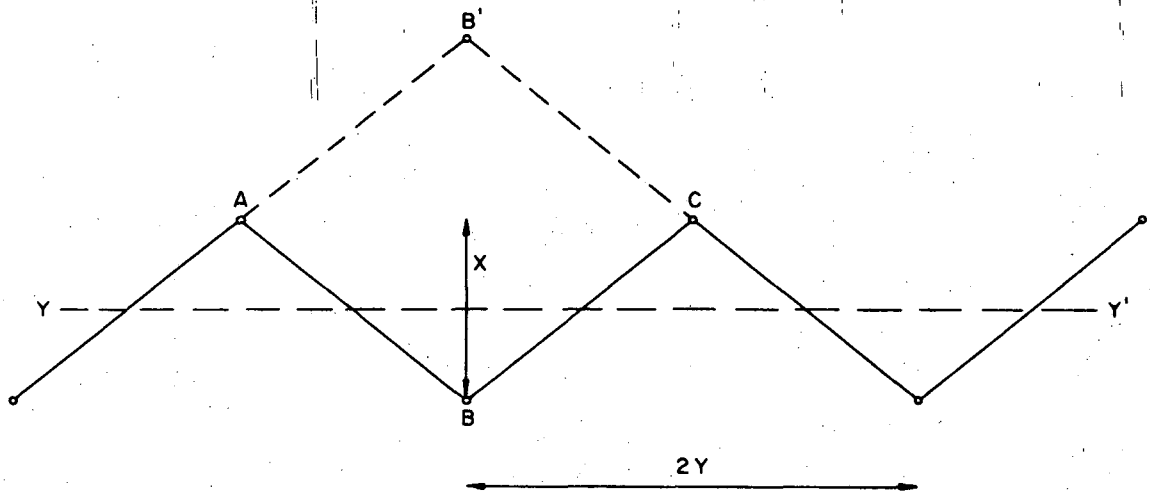

XBL 687-1396

Fig. 6 Friedel's triangular array

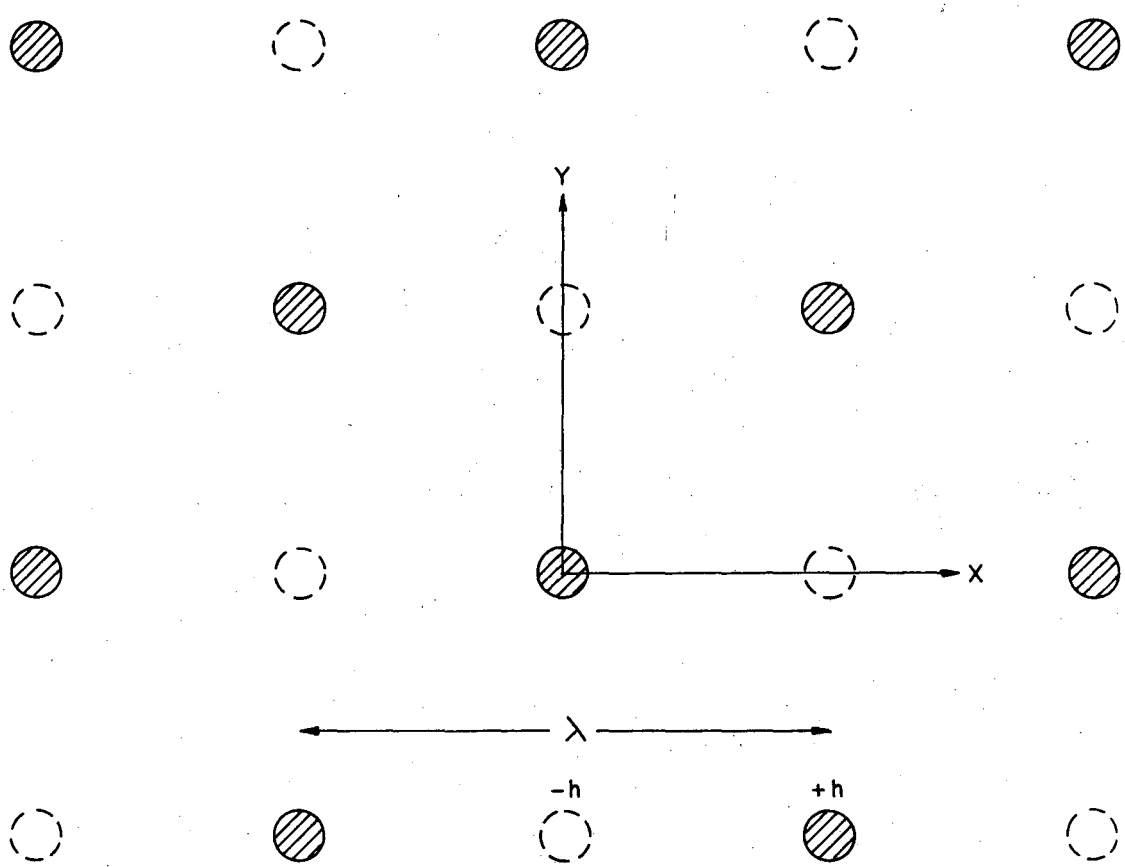

XBL 687-1411

Fig. 7 Array 1

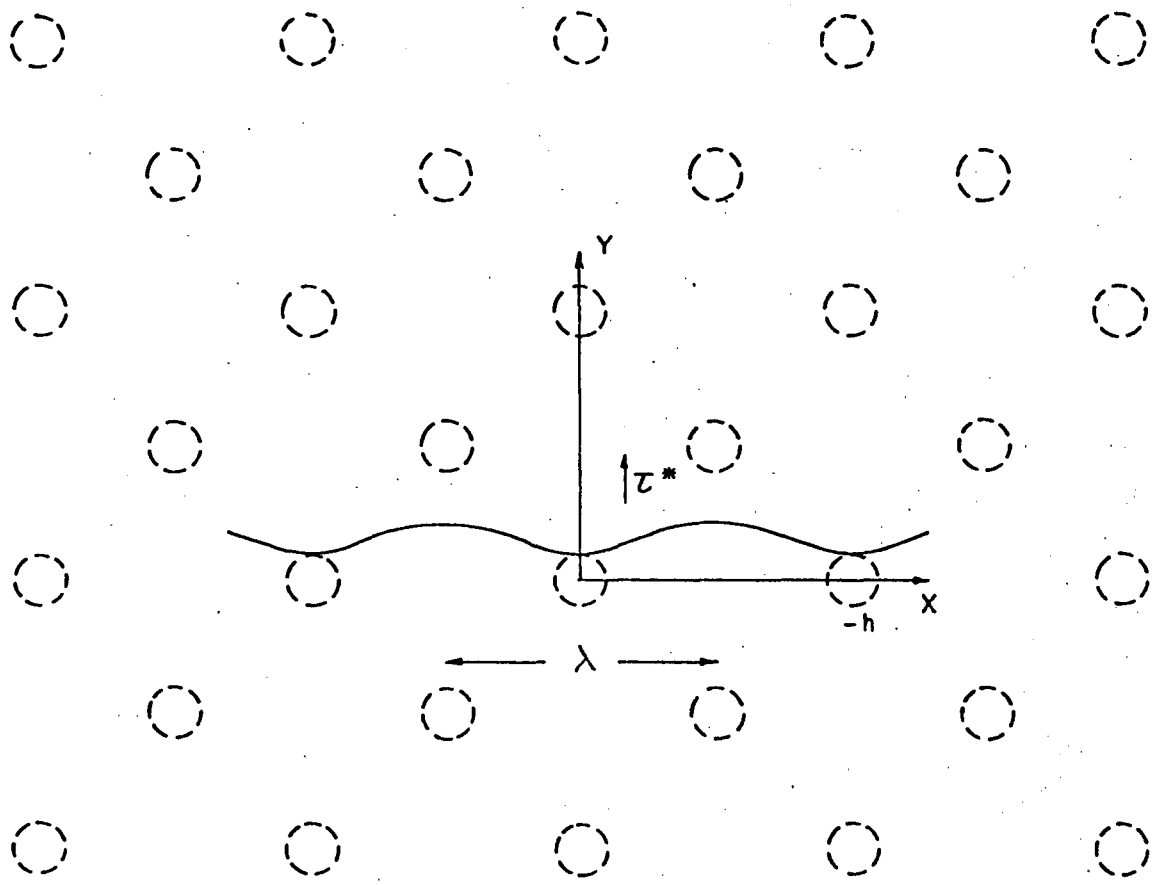

XBL 687-1407

Fig. 8 Array 2

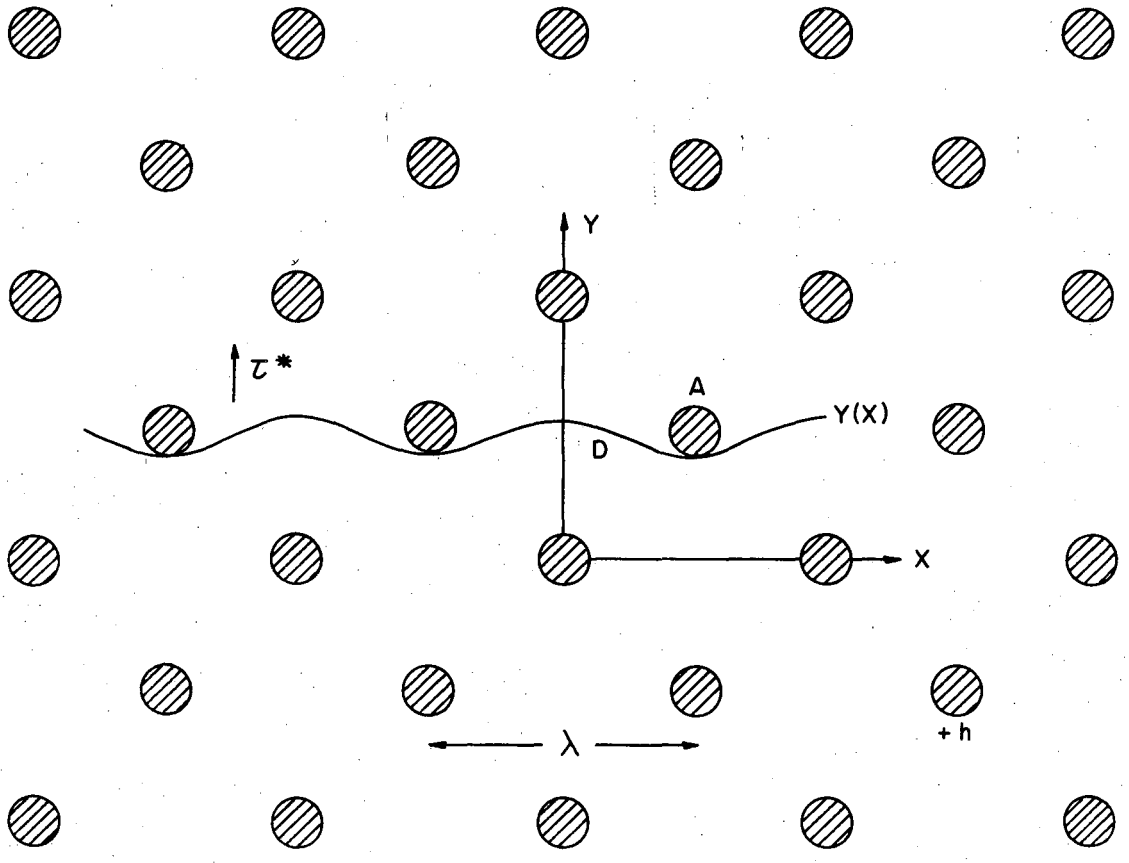

XBL 687-1410

Fig. 9 Array 3

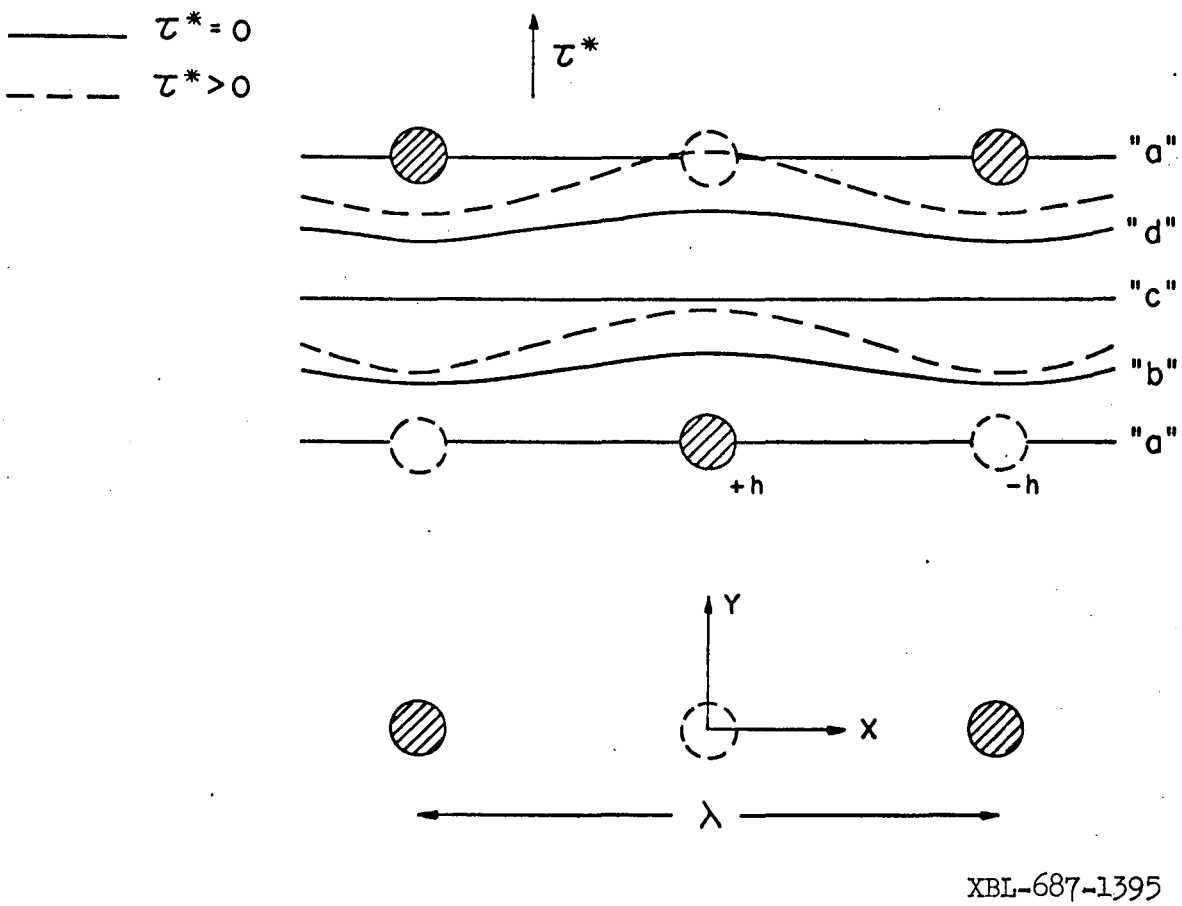

Fig. 10 Periodic configurations in array 1

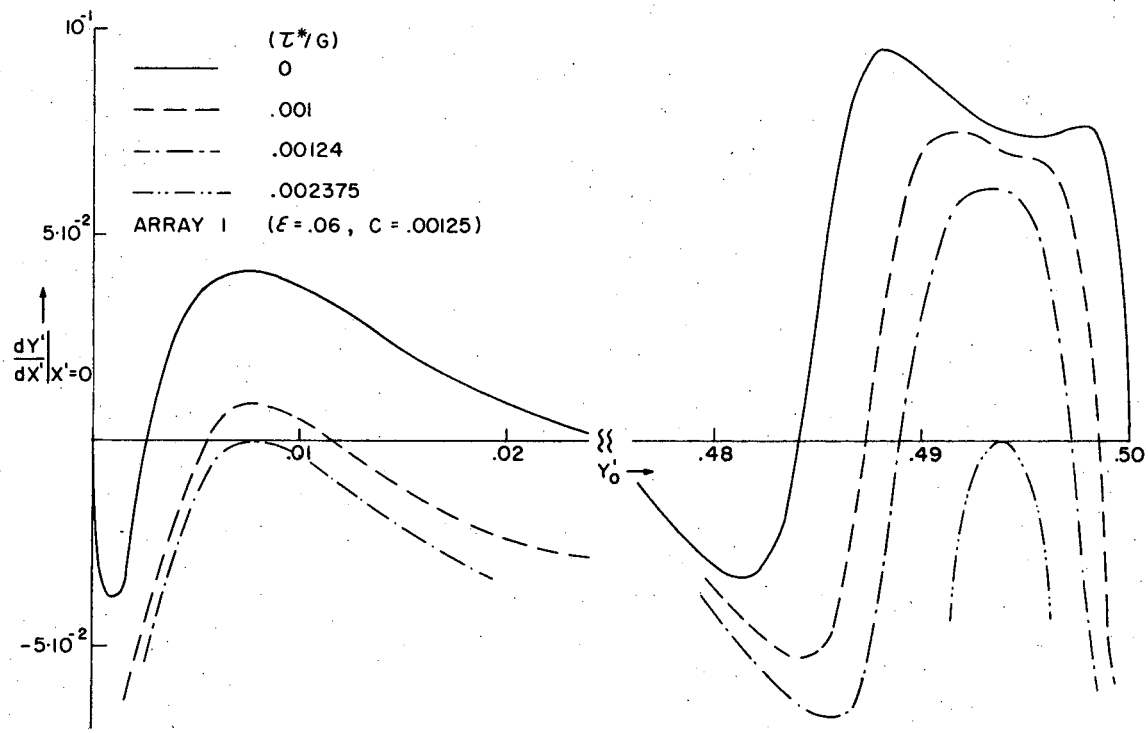

Fig. 11 Displacements satisfying the periodicity condition

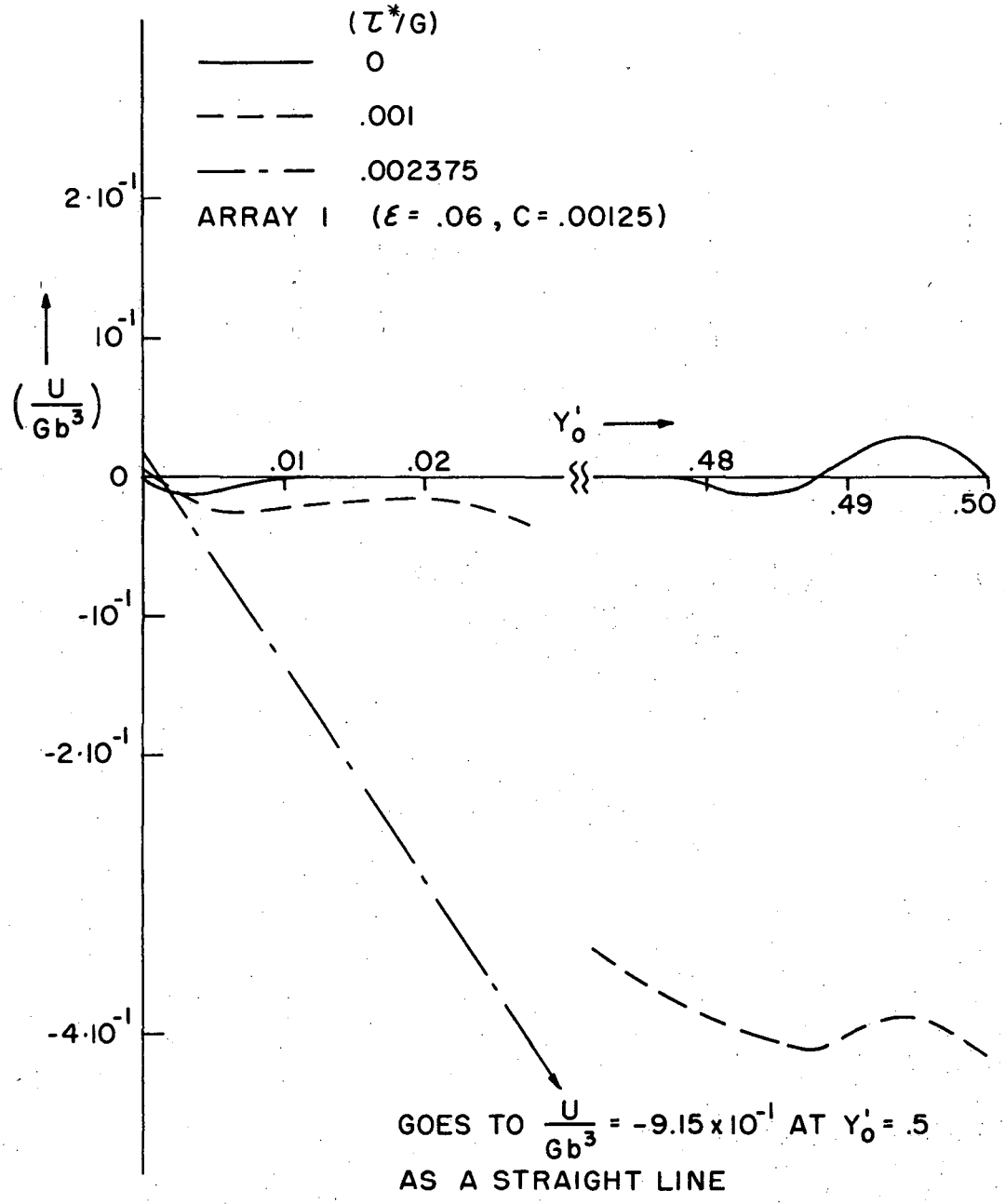

XBL 687-1397

Fig. 12 Minimum energy calculations

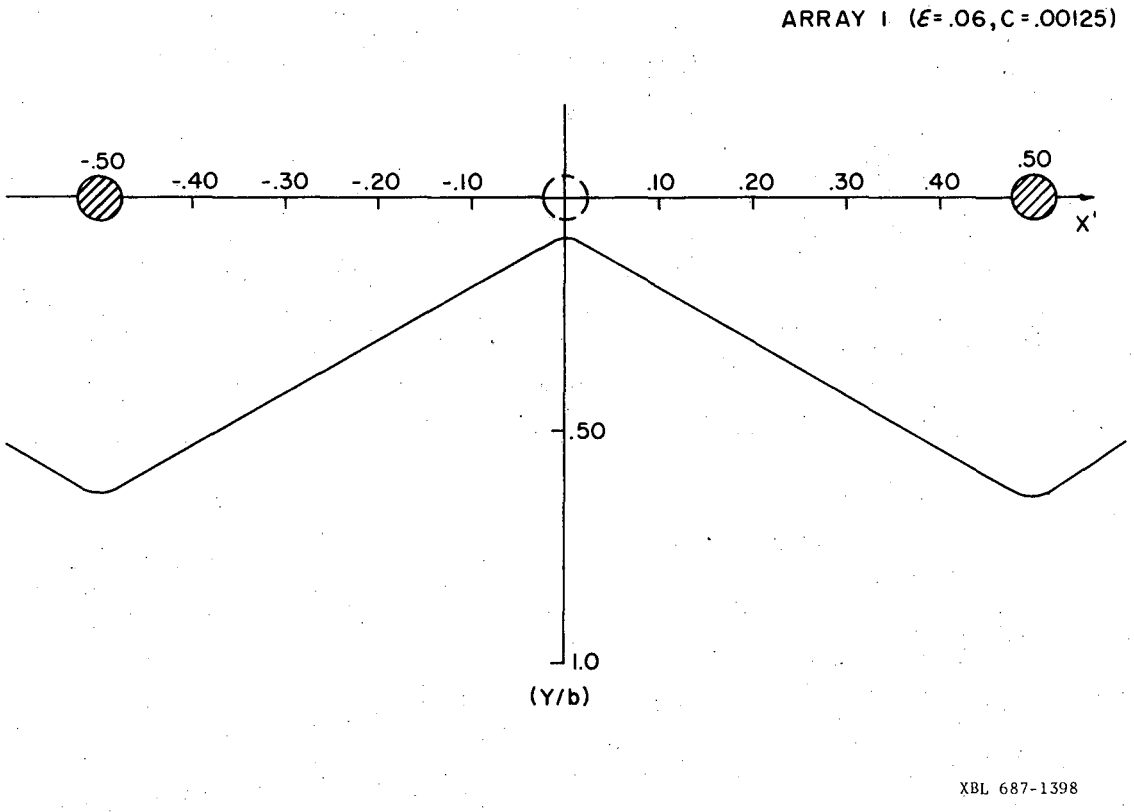

Fig. 13 Equilibrium line shape at zero stress

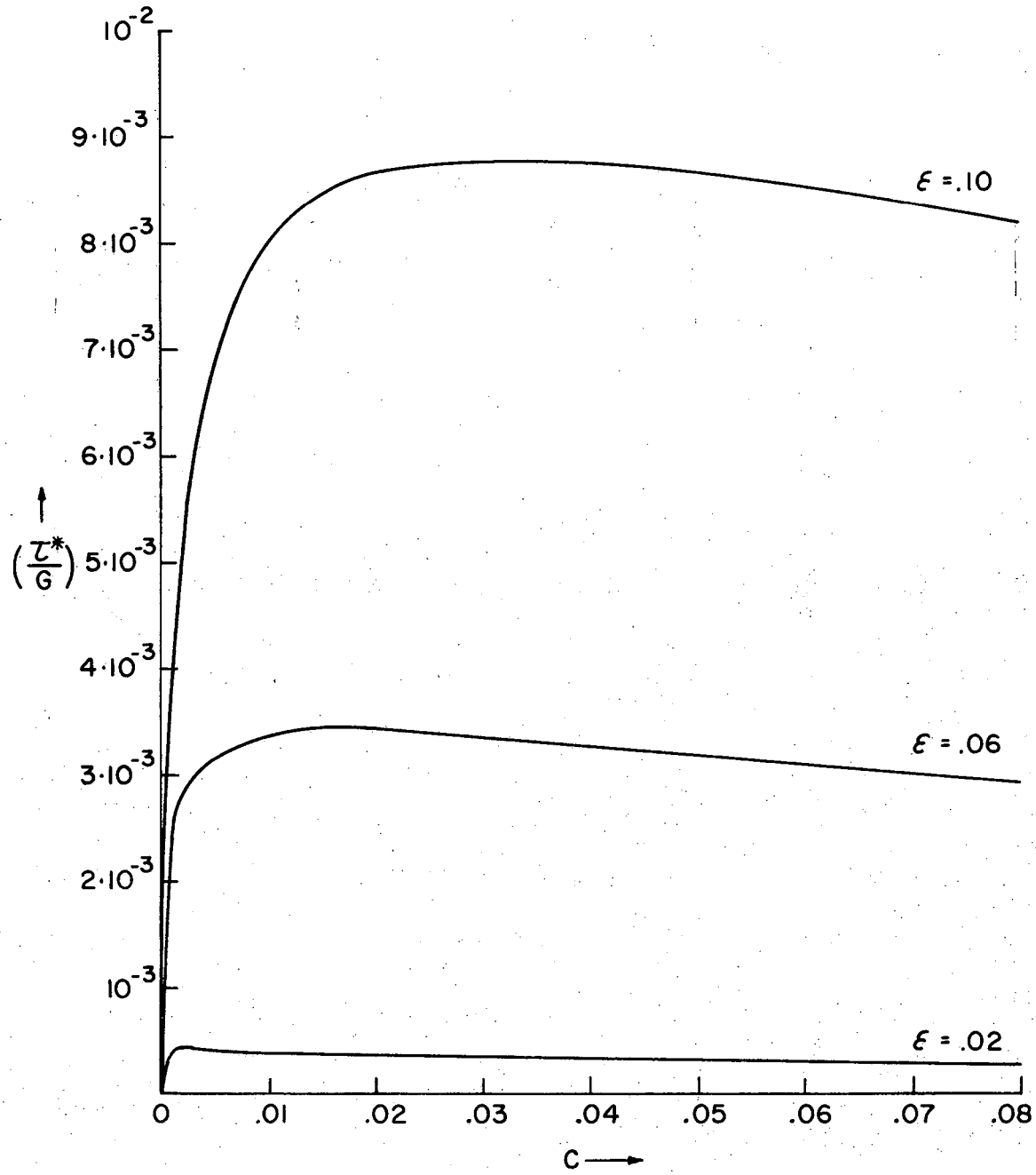

XBL 687-1399

Fig. 14 The flow stress of array 1

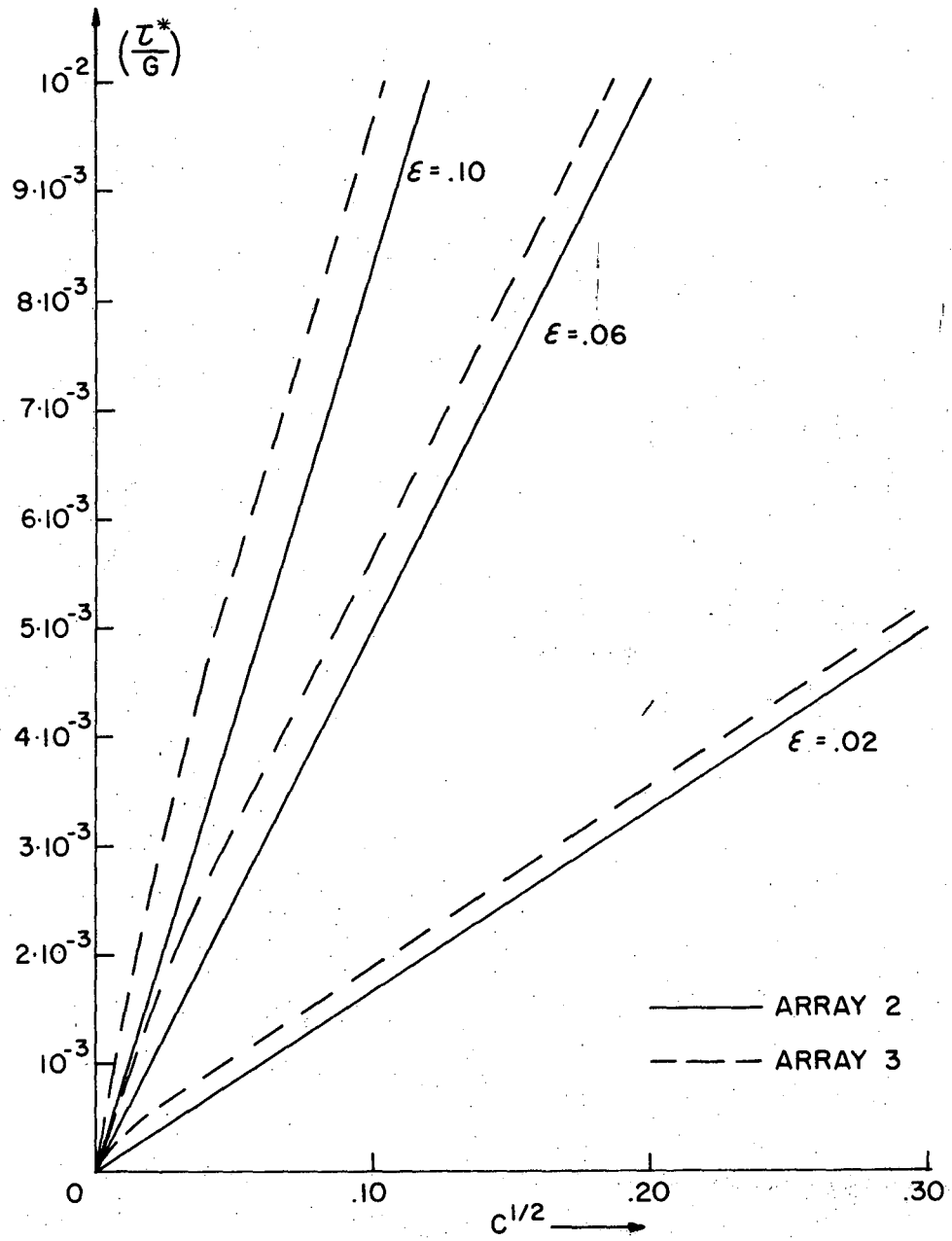

XBL 687-1400

Fig. 15 The flow stress of arrays 2 and 3

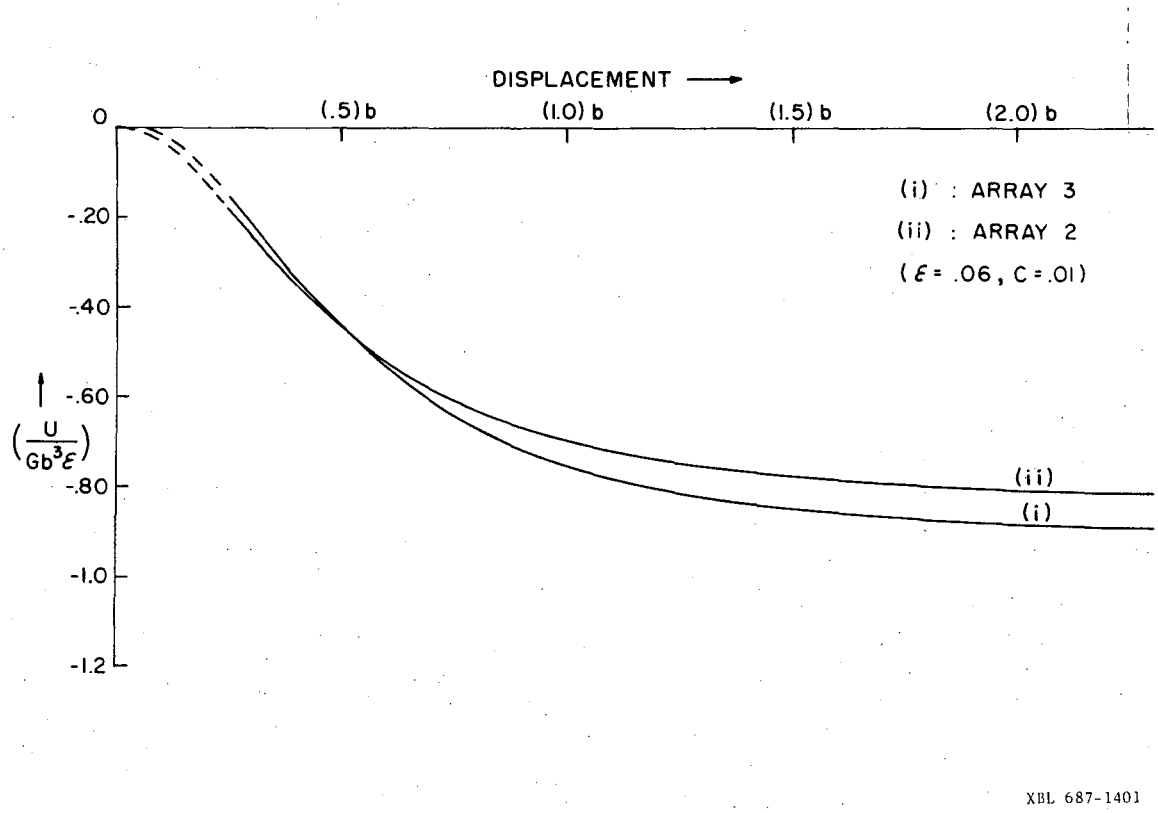

Fig. 16 Strain-energy interaction for flexible dislocations

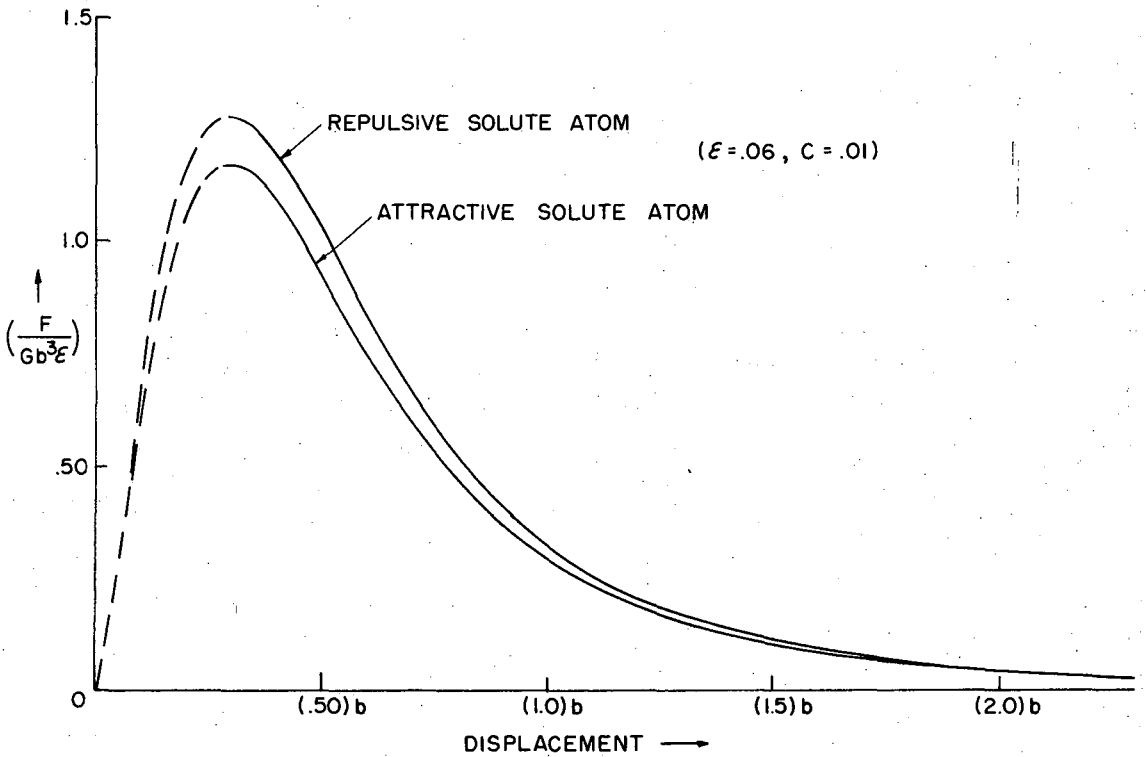

XBL 687-1414

Fig. 17 Force-displacement diagrams for flexible dislocations

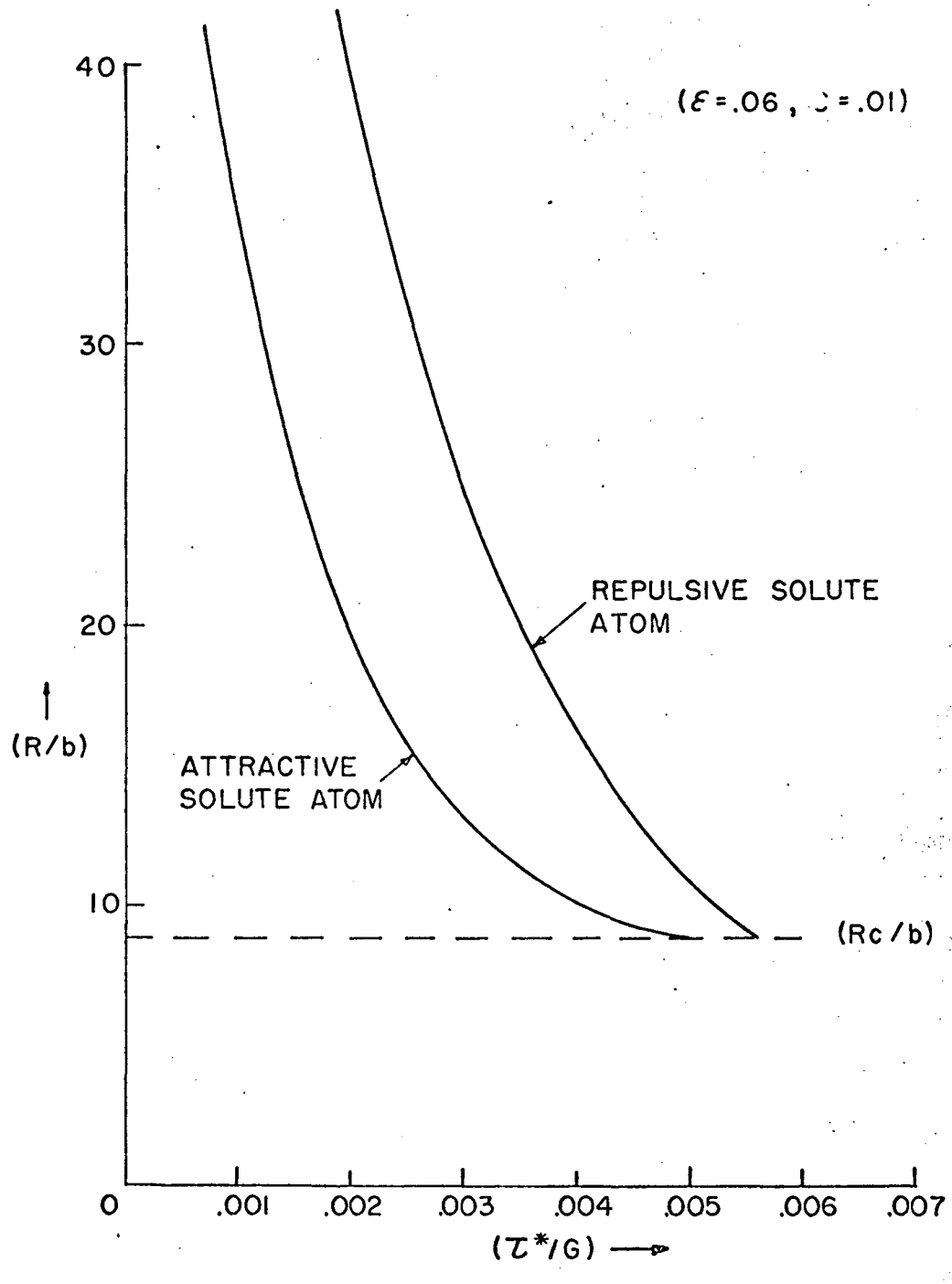

XBL 687-1392

Fig. 18 The equilibrium radius of curvature near a solute atom

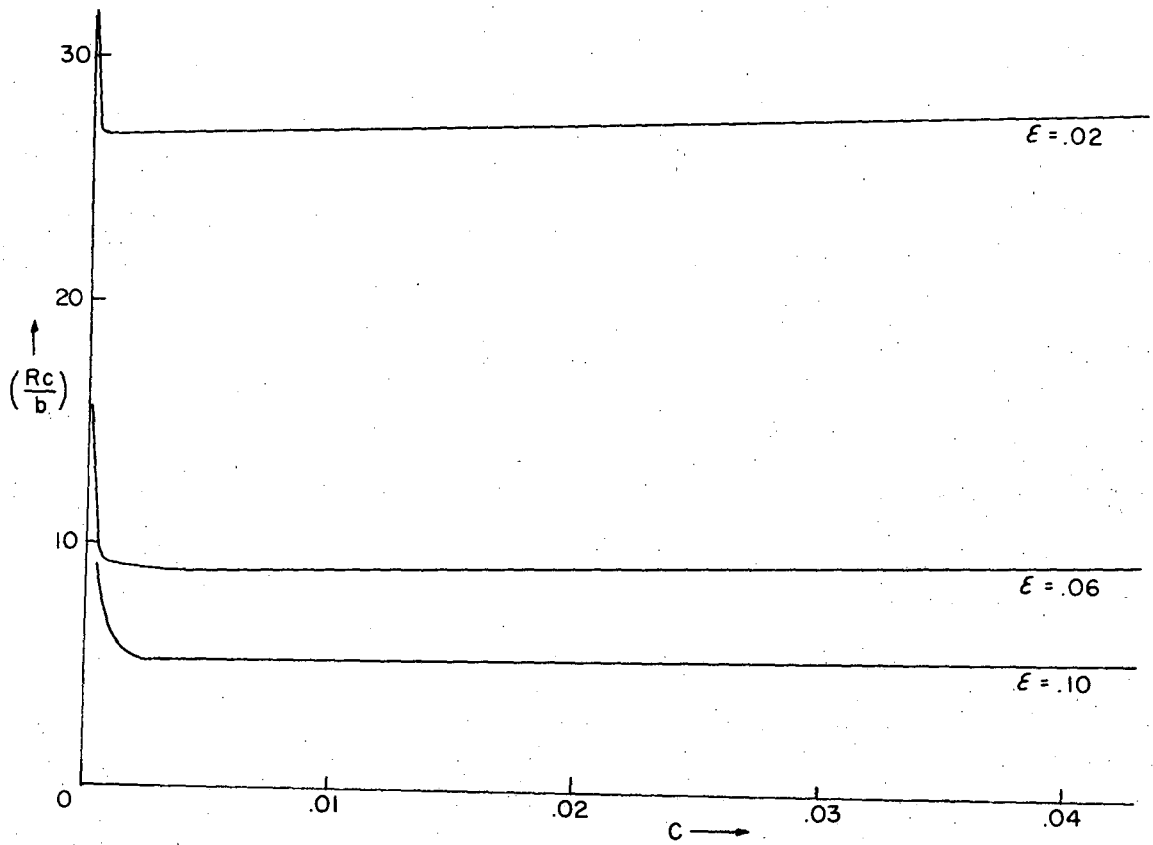

XBL 687-1415

Fig. 19 Critical or cutting radius of curvature

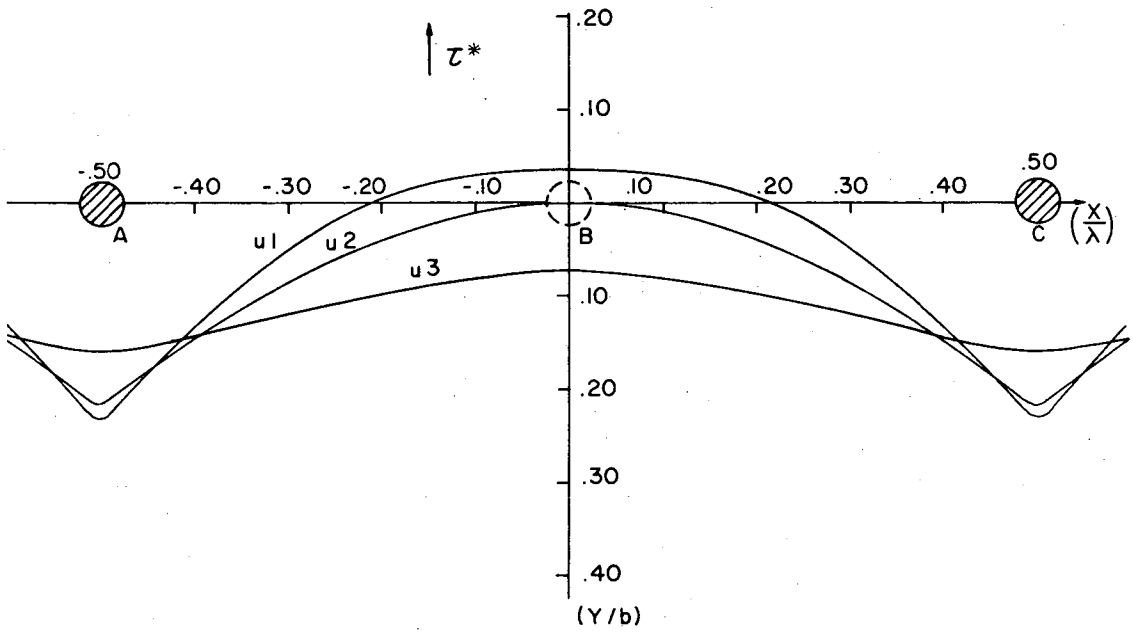

XBL 687-1393

Fig. 20a. Equilibrium line shapes under stress for configuration "d"

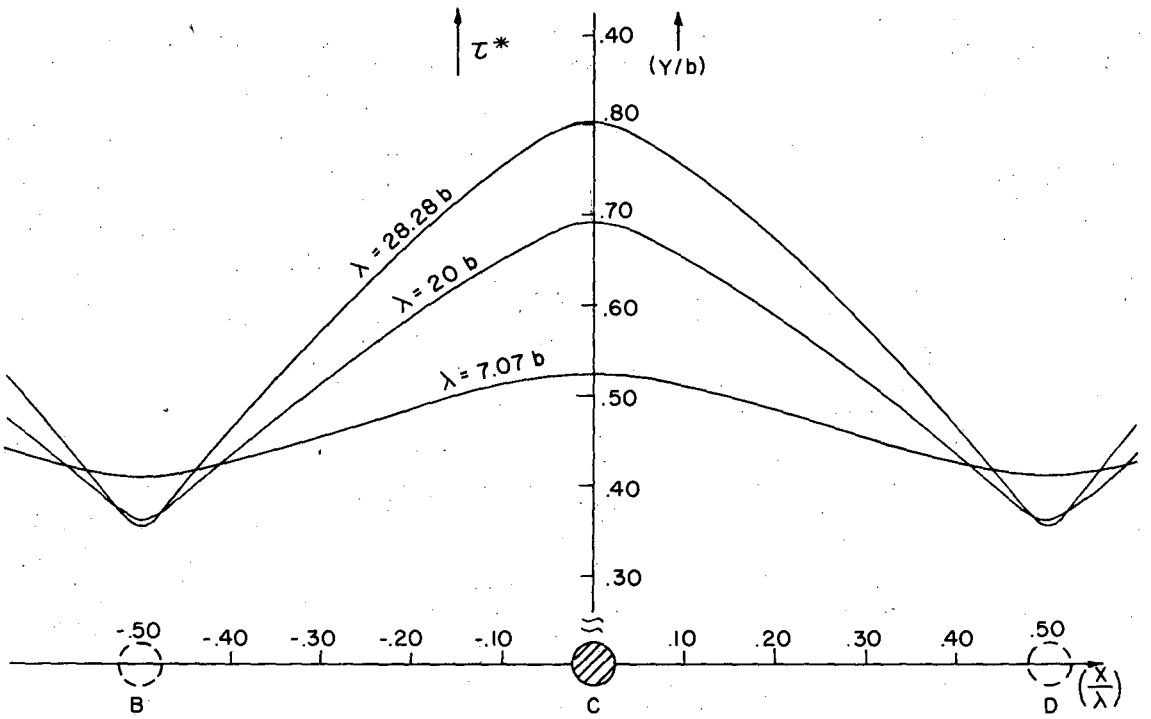

XBL 687-1394

Fig. 20b Equilibrium line shapes under stress for configuration "b"

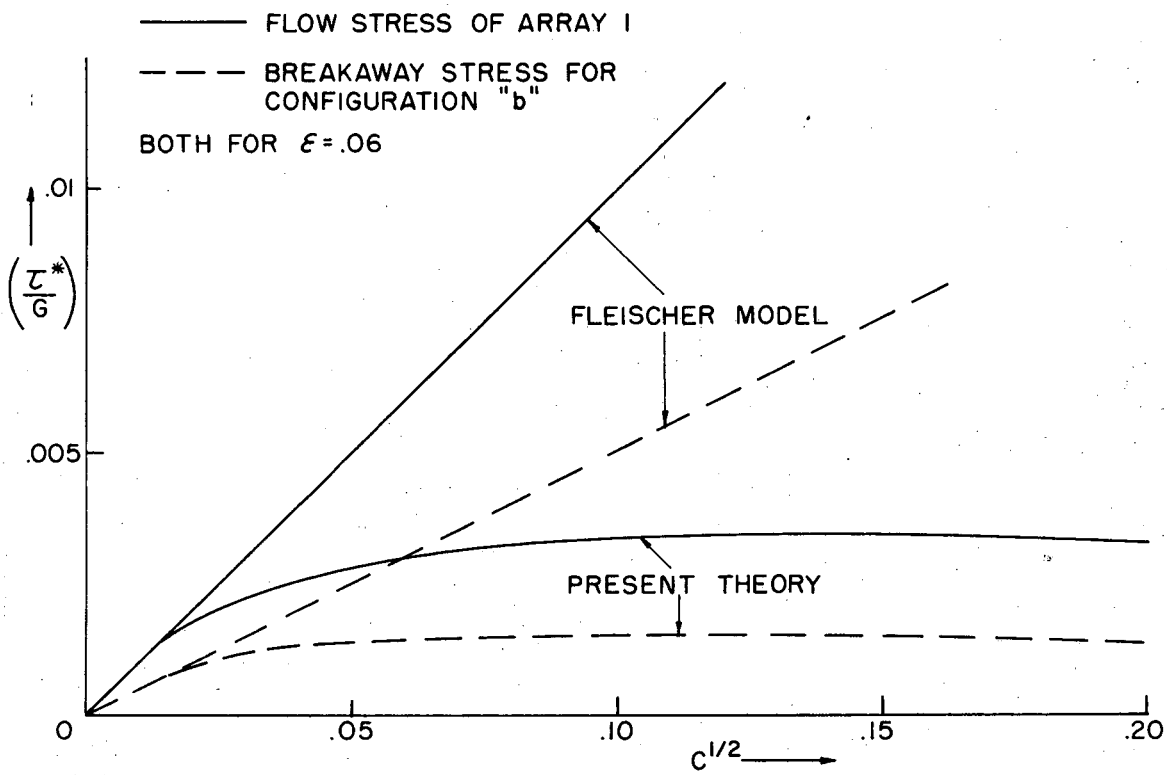

XBL 687-1405

Fig. 21 Critical stresses in array 1

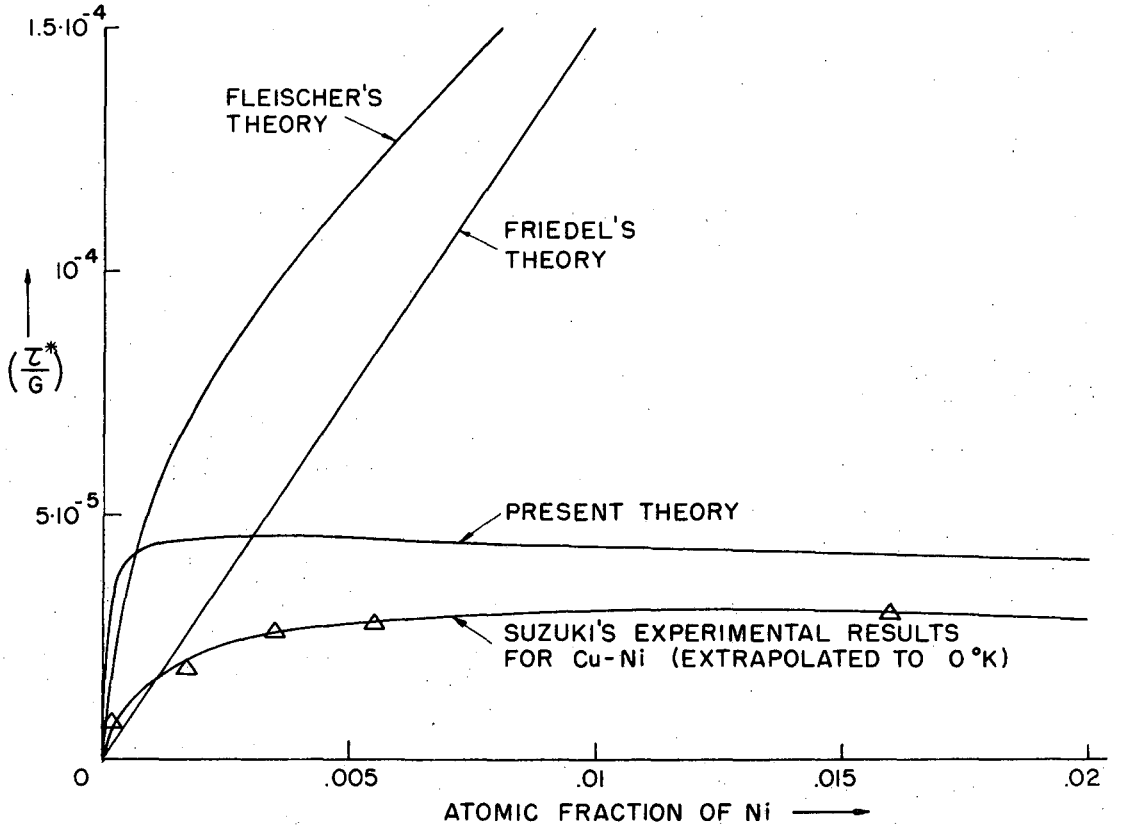

XBL 687-1406

Fig. 22 Comparisons with experimental results

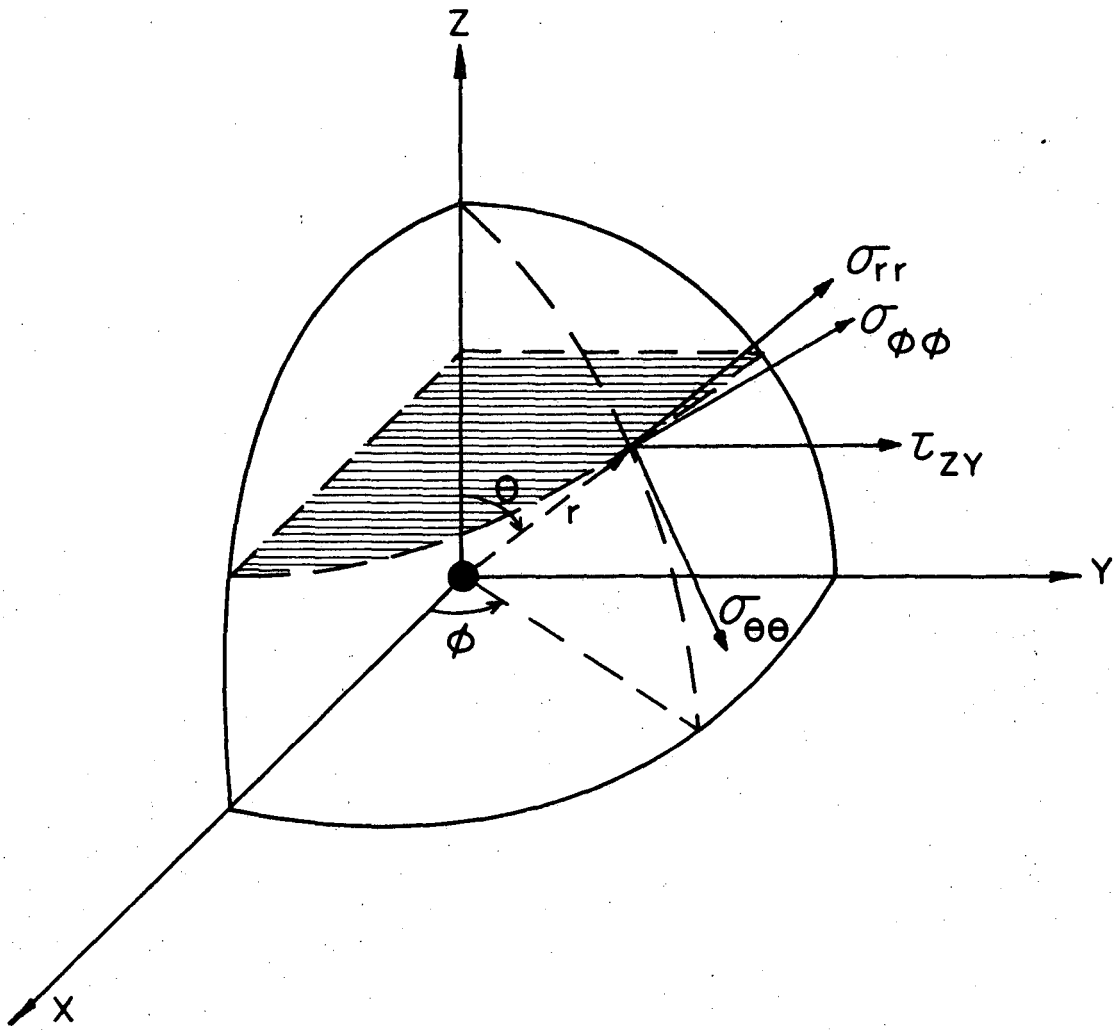

XBL 687-1409

Fig. A-1 Solute atom - slip plane geometry